AFRL-VS-PS-
TR-2004-1049

AFRL-VS-PS-
TR-2004-1049

Advancement of Polymer Detectors for Space Applications

Edward W. Taylor
Tingying Zeng
Richard O. Claus

International Photonics Consultants, Inc.
38 Knife Edge
Pagosa Springs, CO 81147

16 March 2004

Final Report

AIR FORCE RESEARCH LABORATORY
Space Vehicles Directorate
3550 Aberdeen Ave SE
AIR FORCE MATERIEL COMMAND
KIRTLAND AIR FORCE BASE, NM 87117-5776

DTIC COPY

AFRL-VS-PS-TR-2004-1049

Using Government drawings, specifications, or other data included in this document for any purpose other than Government procurement does not in any way obligate the U.S. Government. The fact that the Government formulated or supplied the drawings, specifications, or other data, does not license the holder or any other person or corporation; or convey any rights or permission to manufacture, use, or sell any patented invention that may relate to them.

This report has been reviewed by the Public Affairs Office and is releasable to the National Technical Information Service (NTIS). At NTIS, is will be available to the general public, including foreign nationals.

If you change your address, wish to be removed from this mailing list, or your organization no longer employs the addressee, please notify AFRL/VSSS, 3550 Aberdeen Ave SE, Kirtland AFB, NM 87117-5776.

Do not return copies of this report unless contractual obligations or notice on a specific document requires its return.

This report has been approved for publication.

//signed//

DANG LE, Capt, USAF
Project Manager

//signed//

KIRT S. MOSER, DR-IV
Chief, Spacecraft Technology Division

REPORT DOCUMENTATION PAGE

Form Approved
OMB No. 0704-0188

1. REPORT DATE *(DD-MM-YYYY)*	**2. REPORT TYPE**	**3. DATES COVERED** *(From - To)*
16-03-2004	Final Report	September 2002 – March 2004

4. TITLE AND SUBTITLE
Advancement of Polymer Detectors for Space Applications

5a. CONTRACT NUMBER
F29601-02-C-0254

5b. GRANT NUMBER

5c. PROGRAM ELEMENT NUMBER
62601F

6. AUTHOR(S)
Edward W. Taylor
Tingying Zeng*
Richard O. Claus*

5d. PROJECT NUMBER
4846

5e. TASK NUMBER
CR

5f. WORK UNIT NUMBER
A1

7. PERFORMING ORGANIZATION NAME(S) AND ADDRESS(ES)

International Photonics Consultants, Inc.
38 Knife Edge,
Pagosa Springs, CO 81147

*Nanosonic, Inc.
1485 South Main Street
Blacksburg, VA 24060

8. PERFORMING ORGANIZATION REPORT

9. SPONSORING / MONITORING AGENCY NAME(S) AND ADDRESS(ES)
Air Force Research Laboratory
Space Vehicles Directorate
3550 Aberdeen Ave., SE
Kirtland AFB, NM 87117-5776

10. SPONSOR/MONITOR'S ACRONYM(S)

11. SPONSOR/MONITOR'S REPORT NUMBER(S)
AFRL-VS-PS-TR-2004-1049

12. DISTRIBUTION / AVAILABILITY STATEMENT
APPROVED FOR PUBLIC RELEASE; DISTRIBUTION UNLIMITED.

13. SUPPLEMENTARY NOTES

14. ABSTRACT

Photovoltaic polymer detectors incorporating Indium Phosphide (InP) and Cadmiume Selenide (CdSe) quantum dots (QDs) were fabricated, characterized for their open circuit voltage and short circuit currents and studied for radiation resistance. InP QD detectors exhibited higher photovoltages and responded further into the near-IR compared to CdSe QD detectors, however, the CdSe QD detectors exhibited higher external quantum efficiencies than InP QD detectors. InP QD detectors showed excellent resistance to gamma-ray and 25.6 MeV protons at a total dose of ~ 150 krad(si), while CdSe QD PPDs irradiated by gamma-rays to 152 krad (Si) damaged more from environmentally-induced aging effects than by ionization-induced processes. The data suggest that both InP and CdSe QD polymer detectors have excellent resistance to irradiation since strong carrier confinement and lifetimes inherent in QDs reduce the interaction with native defect and nuclear caused dislocations compared to conventional quantum well detectors where carriers have greater mobility and can interact freely with recombination centers.

15. SUBJECT TERMS
Quantum Dot Polymer Photodetectors, Photovoltaic Detectors, Near-IR Detectors, Radiation Resistance, Radiation Hard Detectors, Space Environments, Gamma-Rays, Protons, Space Radiation Effects, InP Quantum Dots, CdSe Quantum Dots

16. SECURITY CLASSIFICATION OF:			**17. LIMITATION OF ABSTRACT**	**18. NUMBER OF PAGES**	**19a. NAME OF RESPONSIBLE PERSON**
					Capt Dang Le
a. REPORT	**b. ABSTRACT**	**c. THIS PAGE**			**19b. TELEPHONE NUMBER** *(include area code)*
Unclassified	Unclassified	Unclassified	SAR	82	(505) 846-2301

Standard Form 298 (Rev. 8-98)
Prescribed by ANSI Std. 239.18

TABLE OF CONTENTS

FIGURES

TABLES

FOREWARD

The objective of this investigation was to advance previous polymer photodetector development investigations accomplished under AFRL/VSSS Contract F29-601-01-C-0261 "Investigation of Radiation Resistant Polymer Photodetectors for Space Applications (Phase I). Specifically, polymer– based photovoltaic detectors incorporating Indium Phosphide (InP) and Cadmium Selenide (CdSe) quantum dot (QD) materials were fabricated, characterized for their open circuit voltage (photovoltage) and short circuit currents and studied for their resistance to irradiation by gamma-rays and high energy protons. The investigation presented a challenge since the least evolved component of the polymer based technologies for lightwave applications is that of the optical detector, especially polymer photodetectors (PPDs) that are required to operate in the near infrared (near-IR).

In Phase I liquid (photoelectrochemical solar cell) and solid-state (nanocrystalline) PPDs were fabricated and evaluated for their potential to function in ionizing radiation. The designs for the PPDs were based on photovoltaic solar cell research reported by the Laboratory for Photonics and Interfaces at the Swiss Federal Institute of Technology in Lausanne, Switzerland. Gamma-ray data resulting from the irradiation of solid ruthenium (Ru) complex dye and titanium dioxide (TiO_2) nanoparticle detectors to 100 krad(Si) total dose in Phase I, exhibited a potential for saturation of the detector photovoltage degradation. The Phase II investigation centered on replacing the Ru sensitizer with InP and CdSe quantum dots (QDs) in order to demonstrate the potential for extending the polymer photodetector wavelength response to the near-IR (i.e. ~ 1000 nm). The use of appropriate QDs also provided a potential for enhancing the radiation resistance of the PPDs.

Bandgap- engineered polymer materials are important for advancing next-generation ultra-miniature, high bandwidth, cost effective photonic, optoelectronic and electrooptic technology for space applications. Molecular engineering can be used to achieve selective orientation of π-electrons within the polymer structure and change the index of refraction The degree of birefringence and nonlinear properties can also be altered in many

polymeric materials to eventually fabricate efficient and economical light emitting diodes, lasers, optical waveguides modulators and detectors. The ability to molecularly manipulate the polarization and refractive index as well as the spectral absorption and charge transfer efficiencies in polymer materials is important for realizing efficient and useful near-IR photodetectors and optical signal conditioning devices such as modulators and polarizers.

The development of polymer-based detectors are very important to the space community since they potentially offer many advantages compared to their inorganic counterparts, including: reduced size and weight, very low manufacturing costs, high yields, robust structures, and most importantly, flexible plastic-like arrays that will have widespread potential for applications to next-generation DOD and commercial space systems. While atmospheric, exo-atmospheric, atomic oxygen scavenging, dielectric charging, electromagnetic interference, temperature, vacuum and radiation induced degradation effects are well known in many inorganic electronic materials and components, an understanding of the physics of interactions caused by ionizing radiation in polymeric based optical and electronic devices are virtually nonexistent.

Conclusive data demonstrating emerging polymeric materials' resistance to ionizing radiation is critical for eventually applying the technology to space systems. The current lack of a radiation effects data base and absence of rigorous and predictive models for assisting hardened polymer photonics device system designs, best describes the current state-of-the-art. This investigative approach and data resulting from this Phase II effort addresses and responds to these critical issues.

Early and parallel investigations of the interaction of ionizing radiation with polymer device development provides insight and valuable empirical data for rapidly evaluating the radiation resistance of promising radiation resistant technology thereby eliminating costly post-development investigations for determining and implementing radiation hardening mitigation processes. The empirical results reported in this document provide a

first but critical step in addressing these and other concerns essential for developing radiation resistant PPDs for space applications.

ACKNOWLEDGEMENTS

The "Advancement of Polymer Photodetectors for Space Applications" project was directed by Lt. Dang Le of the AFRL Space Sensing & Vehicles Control Branch (VSSS) within the AFRL Space Vehicles Directorate at Kirtland AFB, NM. Lt. Le and Dr. David Cardimona of AFRL/VSSS provided valuable technical contributions throughout the investigation which greatly contributed to the success and objectives of the research study. The fabrication of the QD (nanocrystal) PPDs as well as the pre-and post irradiation measurements were performed by Drs. Tingying Zeng and Richard O. Claus of NanoSonic, Inc, Blacksburg, VA. Mr. Donald Berry of the Sandia National Laboratory Gamma-Ray Irradiation Facility, Kirtland AFB, NM; and Ms. Linda R. Taylor of the International Photonics Consultants (IPC), provided valuable assistance in performing the gamma-ray irradiations of InP - and CdSe-doped QD PPDs . The assistance of Dr. Carlos Casteneda at the University of California Crocker Nuclear Laboratory was most helpful in conducting the high energy proton irradiation of the InP-doped QD PPDs.

1.0 SUMMARY

1.1 Motivation

The research investigation conducted by the International Photonics Consultants, Inc., for the Air Force Research Laboratory Space Sensing & Vehicle Control Branch (VSSS) consisted of the fabrication and characterization of state-of-the-art polymer photodetectors and an evaluation of their responses to gamma-ray and proton irradiations. PPDs were fabricated incorporating InP and CdSe QD (nanocrystal) materials for the purpose of extending the detector response to longer wavelengths. Nanocrystalline InP solutions resulting in QDs varying in size between ~2-10 nm were prepared, integrated into the polymer matrix and observed to strongly absorb light over the range of 330-620 nm with decreasing absorption extending to ~ 1000 nm. Similar processes were used to integrate ~4 nm spherical CdSe quantum dots acquired from an external source into the CdSe QD PPDs for irradiation studies.

The rationale for introducing II-VI and III-V semiconductor QDs into the detector composition matrix was to replace the photo-sensitive dye [ruthenium (Ru) complex] used in solid polymer photodetectors developed by Nanosonic during the first phase of this investigation. Various response models have been proposed to explain the mechanism for the absorbance in QDs, including an electron-hole exchange interaction wherein an exciton state is split into a spin-forbidden triplet state and a higher energy spin-allowed singlet state. Absorption occurs into the upper state followed by relaxation to and light emission from the lower state. The energy difference between the two states is the resonant red shift which corresponds with the desired near-IR performance of the polymer detectors.

Another important reason for incorporating QDs into the polymer matrix was to investigate the potential for increasing the radiation resistance of polymer-based detectors for possible application in ionizing space environments. QDs have been reported to increase the radiation resistance of inorganic lasers and photodetectors. Recent studies have shown that radiation induced damage experienced in QD-doped multiple quantum wells devices is significantly reduced when incorporating QDs. The quantum

confinement aspects of QDs result in efficient carrier capture and exciton localization. QD trapped carriers are thus confined to interacting with defects within the QDs or in proximity to the QDs thereby reducing the non-radiative recombination process. Efficient capture of carriers by QDs is beneficial since carriers remain trapped until combining radiatively. Because of strong carrier confinement, lifetimes in QD doped detectors are much less affected by nuclear radiation-induced ionization and dislocation effects compared to conventional QW detectors where the carriers have greater mobility. Thus, as will be shown, the objectives of investigating and advancing the development of InP and CdSe QD PPDs operating at near-IR wavelengths in the presence of gamma-rays and protons was accomplished in this project.

1.2 QD PPD Performance Results

Polymer photovoltaic detectors incorporating InP QDs exhibited higher open circuit voltages (i.e. photovoltages) and responded further into the near-IR compared to photovoltaic detectors based on CdSe QDs. InP QD PPDs exhibited pre-irradiated photovoltage outputs under laser illumination at λ = 532 nm and 245 mW incident power, ranging from 307-617 mV (peak) Photovoltage responses for sixteen InP QD PPDs were accomplished while illumination of ten CdSe QD PPDs using a solar simulator yielded photovoltages ranging from 304 - 309 mV (8.21 mW/cm^2 at λ = 600 nm), and , 22.7 mV at 900 nm (40.5 mW/cm^2 incident power). InP QD PPDs exhibited near-IR responses to ~ 1000 nm, while the CdSe QD PPDs cut-off occurred at ~ 700 nm. The study was successful in demonstrating that QDs introduced within the polymer matrix shift the detector absorption spectra towards the near-IR. Post-irradiation analysis of the QD PPDs indicated that all samples were degraded by the irradiations, but to different degrees. The pre-and post-irradiation photovoltage outputs varied within sample sets and were attributed in part to inconsistencies in device fabrication such as inhomogeneous dispersal of the QD materials within the PPD composition and in part due to aging. Aging in the context of this report refers to the deterioration of the polymer photovoltaic properties via exposure of the detector constituents to atmospheric effects such as atomic oxygen, moisture and light induced effects. Aging can affect the stability

of PPD photochemistry and photophysical stability of hole transport materials thus reducing the detector charge transport properties.

Compared to the performance of the InP QD PPD devices, the CdSe QD PPD devices were quite unstable. However, the external quantum efficiencies of the pre-irradiated CdSe QD detectors were much higher compared to InP QD detectors. The gamma-ray damage constant for CdSe QD PPDs compared to that of InP QD PPDs is lower by a factor of 2.5, indicating that that the CdSe QD PPDs exhibited greater resistance to gamma-ray irradiations.

1.3 InP QD PPDs Gamma-Ray Irradiation Results

Gamma-ray irradiation of InP QD PPDs to doses of 150.7 – 152.1 krad(Si) resulted in post- irradiation decreases in the photovoltage outputs of two PPD devices ranging from 38.2 - 59.7% respectively, under illumination by a 532 nm laser. However, the post-irradiation results must be considered with respect to the photovoltage output of a non-irradiated control device which decreased by 37.2% at λ = 532 nm via natural aging processes. Thus, the average radiation induced decrease in the InP QD photovoltage output at ~ 151 krad(Si) was determined to be ~ 11.75 % when compensated for the aging-induced decrease in photovoltage output of the control device. This irradiation data suggested inhomogeneity of polymer and QD composition within the InP QD PPD sample as well as the presence of substantial inherent defect centers which can provide unwanted recombination centers.

The results of a six week aging study was conducted under laser illumination of λ = 532 nm and revealed that the photovoltage outputs of the control and irradiated devices continued to decrease exhibiting linear, first and second exponential decays. At the end of the aging period all irradiated devices exhibited terminal photovoltage outputs ranging from 50.1- 61.6 % of their pre-irradiation (initial) photovoltage values. However, the non-irradiated control device exhibited a terminal photovoltage of 32.3% relative to its initial photovoltage output. The aging data suggests that the gamma-irradiation may have assisted in suppressing the aging decay rate in the irradiated devices, as evidenced by the

response of the non-irradiated control PPD compared to the irradiated PPDs. One possible explanation for the suppression of the natural aging rate is that aging effects were offset by trap filling processes activated by the gamma-ray irradiations. Trap filling and the localization of the exciton field by the introduction of QDs into the polymer matrix were believed to have contributed to the radiation resistance of the devices. The degradation processes exhibited by the InP QD PPDs over the dose levels applied were complex, involving two (i.e. native defects and gamma-ray induced color centers) or more competing degradation processes as evidenced by the photovoltage output data for the applied dose and the long term aging study which exhibited a range of photovoltage decay rates varying from linear to second-order exponential behavior.

A second aging study (initiated on Day 75 after the PPDs were fabricated and characterized) followed the laser illumination study ending on Day 42. A solar simulator source was used to illuminate the PPDs and their photovoltage responses examined over wavelengths extending from 400-1000 nm. Contrary to the linear and exponential decays of the photovoltages observed during the first aging study under 532 nm laser illumination, the recovery data suggests that light-induced and room temperature annealing of the irradiated and control device occurred during illumination by the broadband solar simulator. The PPD photovoltages were measured at 100 nm increments from 400-1000 nm and a final photovoltage measurement was performed on the 131st day of the study which showed that all PPDs experienced an increase in their photovoltage outputs relative to their photovoltages measured on Day 75. Since the measurements were made at room temperatures, the data suggests that photo-bleaching induced by the solar simulator source occurred. Typical increases in PPD photovoltage output measured on Day 131 ranged in one device from 91.5 % [at a dose of 152.1 krad (λ == 500 nm) to 55.9 % at 152.1 (λ= 900 nm)]. The photovoltage recovery process was most apparent for devices that were exposed to > 150 krad(Si).

1.4 InP QD PPDs Proton Irradiation Results

The irradiation of InP QD PPDs by 25.6 MeV protons provided contrasting data compared to the gamma-ray results. In general the PPDs underwent greater and

permanent degradation to their photvoltage outputs. This result is not unexpected since protons can cause permanent dislocation effects in addition to transient ionization processes. Illuminated by a 532 nm laser system, the post– irradiation photovoltage for six InP QD PPD samples were observed to decrease exponentially for increasing dose rather than emulating the linear behavior for applied dose as observed for the gamma-ray irradiations.

In contrast to the gamma-ray irradiations, an aging study conducted using the solar simulator revealed that the photovoltage decay with time was accelerated and generally scaled with dose at shorter wavelengths. The photovoltage output of the non-irradiated InP QD PPD control device decreased by 40 mV from its initial characterization measurement (Day 1) of 377 mV, indicating it underwent aging (~10.6%) over the three month time period between pre- and post- irradiation measurements. This modest decrease in photovoltage (compared to the 184 mV photovoltage decrease observed for the InP QD PPDs control device used in the gamma-ray irradiations) suggested that the sample set of InP QD PPDs provided for the proton irradiations were quite stable. Somewhat consistent with the recovery of the photovoltage output exhibited in the non-irradiated control sample used in the gamma-ray studies, slight increases or minimal aging was observed in the control device belonging to the proton studies. The "flatness" of the aging curves at wavelengths 800nm, 900nm, and 1000 nm indicated that photovoltage decay was less pronounced at longer wavelengths.

1.5 CdSe QD PPDs Gamma-Ray Irradiation Results

Gamma-ray irradiation of CdSe QD PPDs indicated a second order exponential growth in photovoltage reduction with increasing dose. At doses < 94.3 krad(Si) the decrease in the photovoltage was similar to photovoltage reductions noted in two non-irradiated control devices. Two CdSe QD PPDS illuminated at λ = 600 nm and irradiated at the highest dose [153 krad(Si)] exhibited photovoltage reductions of 91.4 % and 88.0 %. Pre-irradiation measurements of the short circuit measurements ranged from 5.9 to 12.3 μA, however, short circuit current levels in the irradiated PPDs including the non-irradiated control samples were below the signal/noise resolution of the measurement system. The

increased noise level and suppressed short circuit current was attributed to rapid aging effects experienced by the PPDs, rather than as a result of the post-gamma-ray irradiation. Approximately one month elapsed between the fabrication, photovoltage and short circuit current measurements and, the gamma-ray irradiation measurements. The control CdSe QD PPDs experienced significant aging decay in this short interval resulting in photovoltage decreases of 66.5% and 63.9 % as measured in the two control devices.

Compared to the performance of the InP QD PPD devices, the CdSe QD PPD devices were quite unstable although the initial external quantum efficiencies of CdSe QD detectors were much higher compared to InP QD detectors. The gamma-ray linear damage constant for the CdSe QD PPDs was 0.667 mV / [krad(Si)] compared to [1.64 mV/ krad(Si)] for InP QD PPDs indicating that that the CdSe QD PPDs exhibited greater resistance to gamma-ray irradiations.

2.0 INTRODUCTION

In the previous Phase I study (2000-2001) conducted for AFRL/VSSS by the International Photonics Consultants (IPC) and Nanosonic, Inc. (NS), it was demonstrated that ruthenium complex Ru (N3)/TiO_2 and poly(p-phenylene vinylene)/sulfonated polystyrene (PPV/SPS) PPDs exhibited reductions in their output photovoltages and photocurrents following irradiation by gamma-rays [1,2]. The decreases in photovoltages for all devices were long lived or permanent, with no observed recovery in the time frame of the post-irradiation studies. The pre-and post-irradiation response–behavior varied in identical sample sets and was believed in part due to deterioration of the polymer materials via aging processes evolving from exposure to the ambient atmosphere (atomic oxygen and moisture) as well as photo-induced instabilities. Aging effects can affect the stability of PPD photochemistry and photophysical stability of hole transport materials and thus reduce the detector charge transport properties. In phase I, the PPD deterioration was mainly attributed to less than ideal packaging experienced by some of the samples, allowing (inadvertent) interaction of some samples with the ambient environment.

The photodetector sample size in the Phase I irradiation study was very limited, and a clear interpretation of the ionization–induced effects in the Ru/TiO_2 and PPV/SPS devices proved difficult, especially in determining the scaling response of the PPD output photovoltages with applied dose beyond 100 krad(Si). Certain of the Ru-complex PPD data suggest that a combination of aging and long term if not permanent damage caused by gamma-ray ionization processes was responsible for limiting the ability of the Ru(N2) and Ru(N3) dye molecules to fully regenerate under illumination. Degradation was especially pronounced in liquid PPDs where the data suggested that prolonged relaxation times following pulsed photo-illumination may have resulted from charge trapping and a reduction in the effective conductivity of the charge transport material [1,2]. However, the radiation induced reduction in the output photovoltage for the NanoSonic fabricated Ru(N3) devices appeared to saturate between 51-100 krad(Si) suggesting that the Ru(N3)- devices were potentially resistant to ionizing radiation at higher dose [1,2].

These and other results of the phase I study provided incentive to further investigate the potential for improving PPD performance by chemically modifying the sensitizer component of the PPDs. It was predicted that by using properly sized QDs as the sensitizer, the PPD absorption could be shifted to shorter or longer wavelengths, thus determining the detector spectral wavelength response, a necessity for widespread use in space system applications.

The focus of the Phase II 2002-2003 investigation conducted under Contract F29601-02-C-0254 (Advancement of Polymer detectors for Space Applications) and under the 2003-2004 cost sharing contract modification "Testing of Quantum Dot Polymer Detectors for Space Applications (P0002)" is reported herein. An investigation of polymer based photovoltaic detectors fabricated with InP and CdSe QD materials was conducted. The InP QD PPDs successfully exhibited wavelength shifts to the near IR (< 1000 nm) and were investigated for their responses when irradiated by energetic (25.6 MeV) protons (p^+) at a fluence of ~ 10^{11} p^+/cm^2, and gamma-rays to 150 krad(Si) total dose. Extensive studies of the irradiated and non-irradiated devices conducted over a period of several months successfully differentiated and have first demonstrated the effects of natural aging and radiation induced effects in InP QD PPDs and CdSe QD PPDs. The investigation of CdSe QD PPD devices has shown that compared to the InP QD PPD devices aging effects in CdSe QD PPDs were much greater. However, the external quantum efficiencies of the pre-irradiated CdSe QD detectors were much higher compared to InP QD detectors.

3.0 DESIGN AND FABRICATION OF QD POLYMER-BASED PHOTODETECTORS

3.1 Role of QDs in Determining PPD Near-IR Absorption Responses

Photovoltaic cells based on wide bandgap oxides nanocrystalline semiconductors and sensitized by molecular dyes, have attracted recent attention in design of high performance solar cells [3-6]. Nanocrystalline TiO_2 is of particular relevance for fabricating dye-sensitized photovoltaic cells, where light absorbing materials generate electron-hole pairs and the electrons are collected by the TiO_2. Efficient separation and transport of the oppositely charged carriers is important for charge collection at the device electrodes. In the Phase I study, the PPD light absorbing material consisted of a NS synthesized Ru(N3) which did not exhibit efficient photovoltage response in the near-IR. In the Phase II study, QDs replaced the Ru (N3) sensitizer used in the Phase I study.

By incorporating appropriate size InP QDs into the polymer matrix, a shift of the PPD wavelength response towards the near-IR (800 - 1000 nm) was predicted. It was determined that an InP QD size of ≥ 6 nm would be required for increasing the QD optical absorption into the near-IR regions [5-8]. Various models have been proposed to explain the mechanism for the absorbance in QDs, including an electron-hole exchange interaction model, where an exciton state is split into a spin-forbidden triplet state and a higher energy spin-allowed singlet state [7-9]. Absorption occurs into the upper state followed by relaxation to and light emission from the lower state. The difference between the two states is the resonant red shift. As will be shown in the data that follows, the InP QD PPDs did respond in the near-IR but at suppressed photovoltage outputs compared to wavelengths below 800 nm.

3.2 Synthesis and Characterization of InP QD PPDs

In order to realize efficient near-IR polymer detectors high quantum absorptivity - the fraction of photon energy absorbed by the detector leading to excited states and the formation of electron-hole pairs is of paramount importance. In this study, photon absorbing materials composed of II-VI and III-V semiconductor compounds possessing

bandgap energies in the range of ~1.0 to 1.40 eV were investigated corresponding to the desired near-IR absorption band. Specifically, InP and CdSe QD materials were incorporated into the PPD matrix replacing the Ru(N3) dyes developed and used in previous visible-range detectors during the Phase I study. Bulk InP absorbs strongly at a wavelength of 918 nm, has a lower toxicity and displays greater stability compared to CdSe. Therefore, initially our effort was focused on the synthesis and characterization of InP QD PPDs.

In solution, InP QDs, synthesized by NS displayed a brown to gray color variation due to different particle size distributions. The QDs were prepared via the colloidal chemistry method using $InCl_3$ and P as the reactive raw materials and a similar method was used in the preparation of CdSe QDs. The as-synthesized InP QDs were modified by coordinating the solvent tri-n-octylphosphine oxide (TOPO) and tri-n-octylphosphine (TOP) on the QD surface to achieve monodispersion stability. Next, the InP QDs were precipitated using methanol and washed with large amounts of methanol to remove extra TOPO and TOP, and finally, the QDs were dispersed in toluene for characterization and application.

Figure 1a shows a representative TEM image of the NS synthesized InP QDs, confirming that the InP QD particle sizes predominantly ranged from 1.5 nm to 3 nm. There are however, small amounts of the InP QDs with sizes ranging from 4.0 to 4.5 nm, and also a smaller amount of QDs ranging to 6 nm. Statistically the distributions can be represented by an average QD size of 2.5 nm. Figure 1b shows the corresponding UV-visible optical absorption as quite broad extending over the spectral range of 300 nm (4.1 eV) to 620 nm (~2.0 eV).

The strong optical absorption at > 330nm (~3.75 eV) results from InP QDs sizes < 2nm, while small amounts of larger size QDs (4- 4.5 nm) contribute to the tail of the absorption curve extending into the near- IR range [5]. As illustrated in Figure 2, InP QDs with an average size of 6 nm account for the suppressed absorption in the near-IR (800-1000 nm).

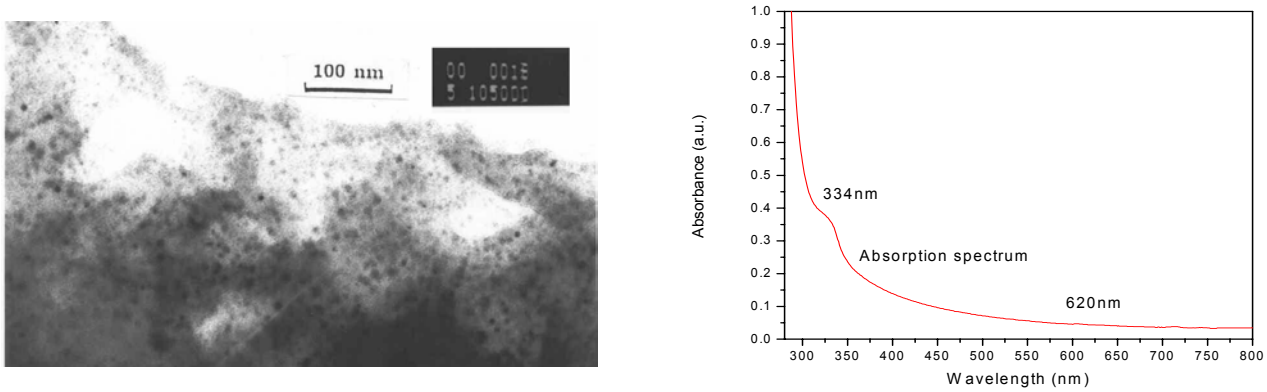

(a) (b)

Figure 1. TEM InP QD image and absorption spectra. In (a) a TEM image of InP QDs synthesized by NanoSonic, Inc is shown and (b) shows the InP QD absorption spectra.

InP QD particle sizes ~ 5-6 nm are necessary for extending or shifting the PPD optical absorption to a potion of the near IR range (800-1000 nm).

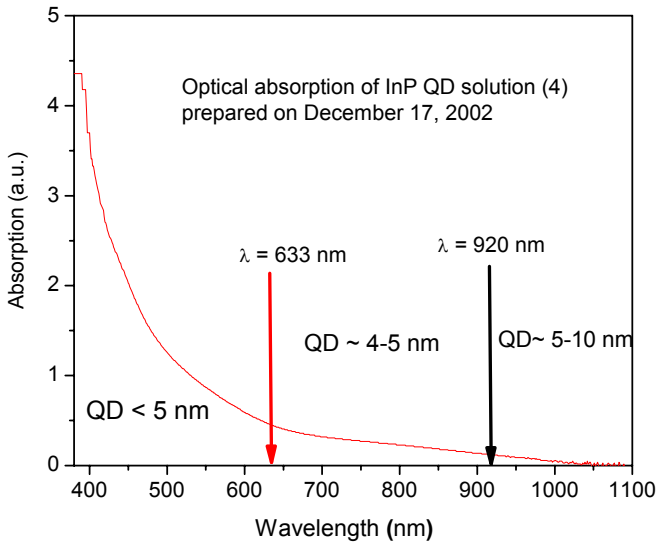

Figure 2. Dependence of optical absorption on InP QD size.

In order to realize stronger absorption within the near-IR, smaller QD sizes would perhaps have to be suppressed and a greater numbers of ~ 6 nm InP QDs would be required for incorporation into the polymer matrix. As shown in Figure 3, UV

illumination of the InP QD solution, caused a color change corresponding to the QD particle size.

Figure 3. InP QD solutions. Without light excitation (brown, left) and with 330 nm excitation (right, slight blue and yellow emissions) were observed in two different particle size solutions.

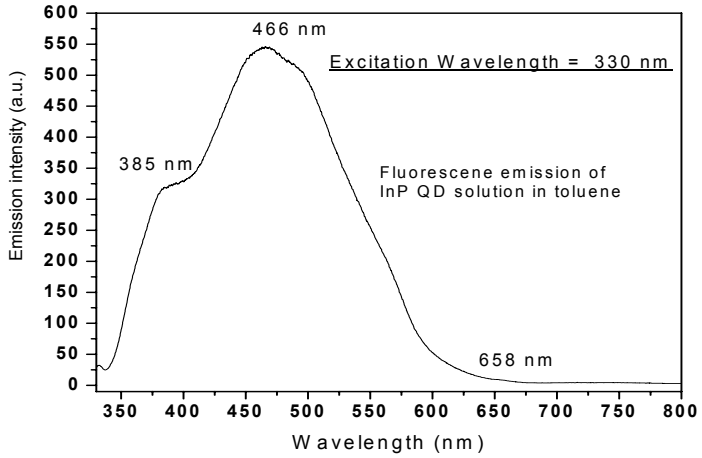

Figure 4. Fluorescence of InP QDs in toluene solution.

QD–sensitized PPDs were designed and fabricated by NS incorporating the synthesized InP QDs described above as the photosensitizer, and using anatase TiO_2 nanocrystalline material as the electron collector layer. Spiro-OMeTAD (Figure 5) from COVION

Organic Semiconductors GmbH, with a purity of 99.9% was used as the hole transport material (HTM), and has strong absorption at 390 nm and a glass transition temperature (T_g) of T_g = 120º C. A 0.16 M HTM solution was prepared by stirring the compound in chlorobenzene overnight at room temperature. The solution also contained 0.33 mM of tris(4-bromophenylaminium hexachloroantimonate $N(PhBr)_3SbCl_6$ and 0.15 mM N-lithiotrifluoromethane sulfonimide ($Li[(CF_3SO_2)_2N]$). $N(PhBr)_3SbCl_6$ acts as a dopant, introducing free charge carriers into the HTM by partial oxidation of the OMeTAD. $Li[(CF_3SO_2)_2N]$ provides a positive charge on the surface of the TiO_2 and produces an electrostatic field, thus aiding electron injection from the excited-InP QD to the conduction band of the TiO_2 semiconductor. Addition of $N(PhBr)_3SbCl_6$ also resulted in a color change of the solution from transparent and colorless to dark-purple. The HTM film was next coated onto the InP QD-stained TiO_2 film using the spin coating process.

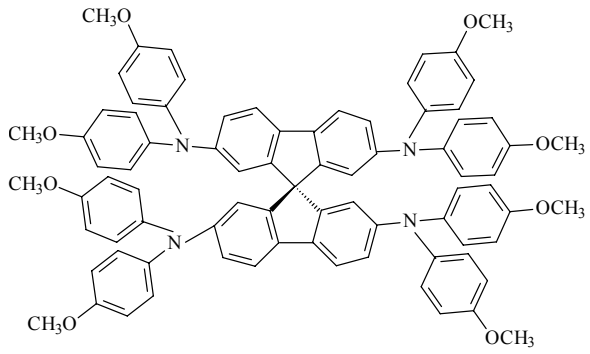

Figure 5. Chemical structure of spiro-OMeTAD.

A counter-electrode composed of an aluminum thin film was applied to the HTM layer using conventional vacuum deposition after drying the HTM layer (in a fume-hood) at room temperature. Figure 6 illustrates the sandwich-structure of the solid polymer HTM-based InP-TiO_2 QD photodetector.

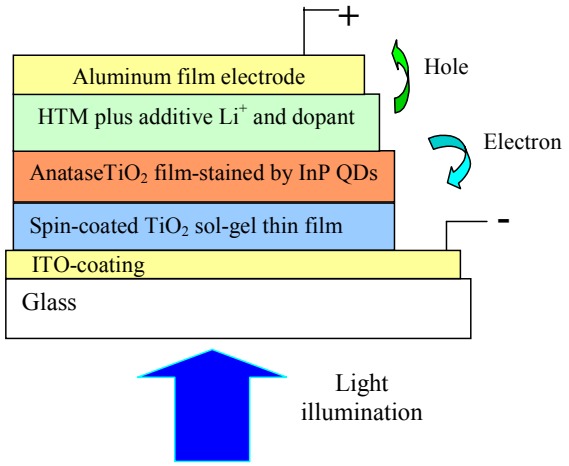

Figure 6. InP QD TiO_2 nanocrystalline-HTM-polymer-based photodetector.

Optical absorption and transmission spectra of the active film with components of TiO_2-InP QD and the HTM are shown in Figure 7 (a) and 7 (b), respectively. As can be seen from the spectra, the ITO-coated substrate has an optical absorption of less than 300 nm,

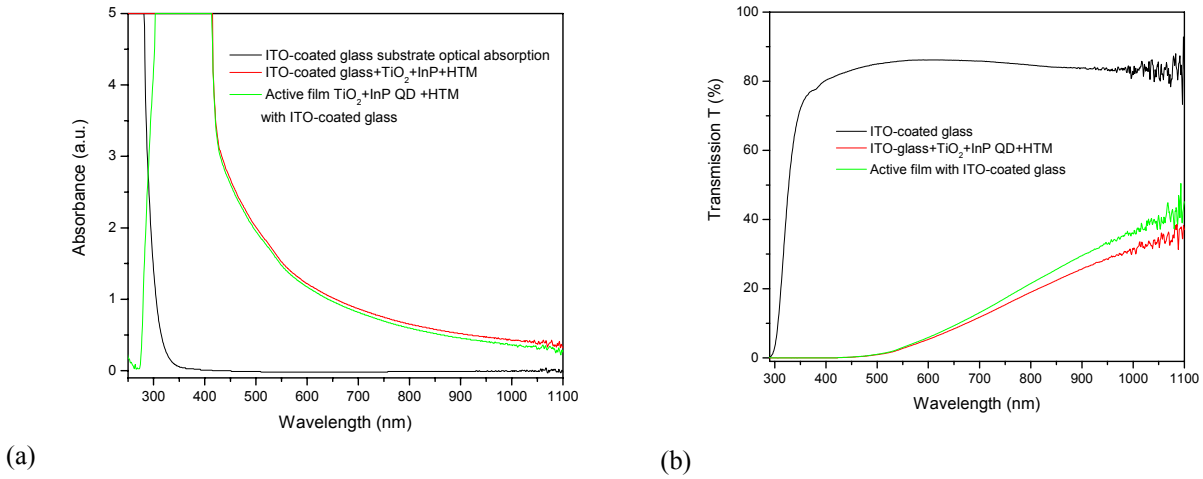

(a) (b)

Figure 7. Optical absorption and transmission in InP QD film. In (a) the absorption in ITO coated glass substrate and HTM is shown. In (b) the optical transmission of InP-QD film, ITO coated glass and HTM is shown.

corresponding to very good transmission above 300 nm. The active film of the InP QD-sensitized TiO_2 PPD exhibited strong absorption in the range of 300 to 500 nm, exhibiting

little or no transmission over this range. Due to the large particle size of the InP QDs, good absorption of the light was also observed between 600nm to 700nm, corresponding to optical transmission loss (T) of T = ~90%. The aluminum film electrode shown in Figure 6 also reflects incident light back into the PPD volume where it again interacts within the detector active regions adding to the absorption process.

3.3 Charge Transfer Processes in QD PPDs

Figure 8 illustrates the principle of photovoltaic signal generation originating in the PPD using QDs as the photosensitizers under excitation by a light source. An ideal QD PPD would result in a device that offered efficient conversion of photons into separated charge carriers with sufficient mobility, long lifetimes and low recombination rates. Under these conditions, collection of charged carriers at opposite device electrodes would be maximized for external circuit use.

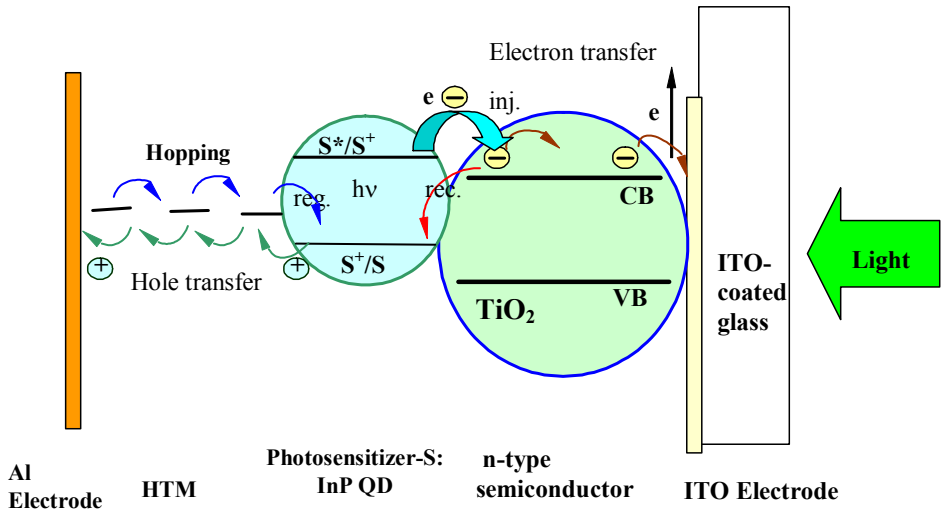

Figure 8. Electron-hole transfer process in an InP QD-TiO_2 nanocrystal heterojunction. Abbreviations are: inj., injection; reg., regeneration; rec., recapture). Shown are the approximate and relative positions of potentials and band energies for the different components.

A brief and simple explanation of the InP QD PPD response under light illumination shown in Figure 8 is as follows: a) light enters the PPD passing efficiently through the transparent glass, the ITO electrode and the TiO_2 nanocrystalline material where it is absorbed by the InP QDs; b) under illumination, the InP QDs absorb energy from the photons and generate excited carriers (electron-hole pairs) which are localized by the quantum dot field; c) the exciton

disassociation at the QD-TiO_2 interface results in the presence of an electric field which separates the charges; d) excited electrons are captured by the TiO_2 nanocrystallites and promoted to the conduction band (if recombination processes are survived) and some electrons reach the InP electrode, while e) holes formed in the disassociation process are transferred by the negatively charged HTM polymer to the aluminum counter electrode; and, f) charges colleted on opposite electrodes provide measurement of a current through a load. for external circuit use.

Figure 9 is a diagram of the experimental setup used for the characterization of the photovoltaic response of InP QD PPDs, specifically photovoltage and photocurrent are measured under illumination by a laser [Figure 9(a)] and solar simulator [(Figure 9(b))]. The active area of the PPD is located between an indium tin oxide (ITO) electrode and a aluminum counter electrode. A resistive load varying from 0.5– 1 Mohm (MΩ) provides photovoltage and photocurrent data which is measured and recorded on an oscilloscope (OSC).

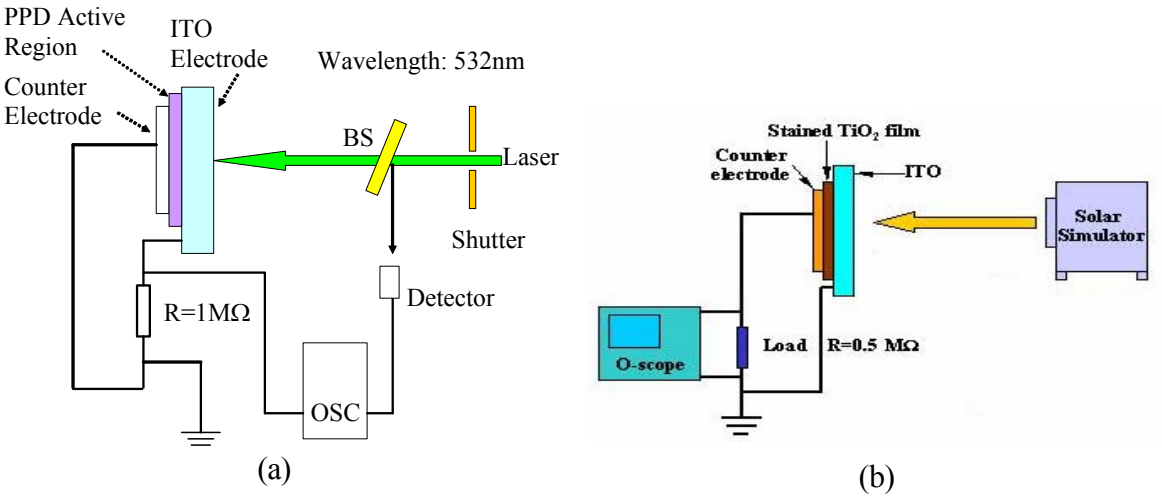

Figure 9. Setup for characterization of PPD photovoltaic performance. In (a) a laser source is used to illuminate the PPD while in (b) a similar set up uses a solar simulator source in place of the laser.

Shown in Figure 10 is a typical photovoltage output response of an InP QD PPD under illumination using a commercial laser source as shown in Figure 9(a). The maximum photovoltage was observed to be 434 mV responding to incident illumination of 245 mW applied over a 5 second interval. The laser beam-waist was 3 mm in diameter and provided 245mW of optical power, illuminating an area on the PPD of 0.071 cm^2. The corresponding photocurrent under these conditions was measured to be 0.012mA/cm^2 with a total load of 0.5 MΩ in the circuit (OSC had a 1MΩ resistance). Under these conditions, the PPD exhibited a short circuit current of 0.098 mA/cm^2 The incident photon-to-electrical current conversion efficiency (IPCE) of the PPD at λ = 532 nm 0.007% (see section 4.7 for calculations of the IPCE).

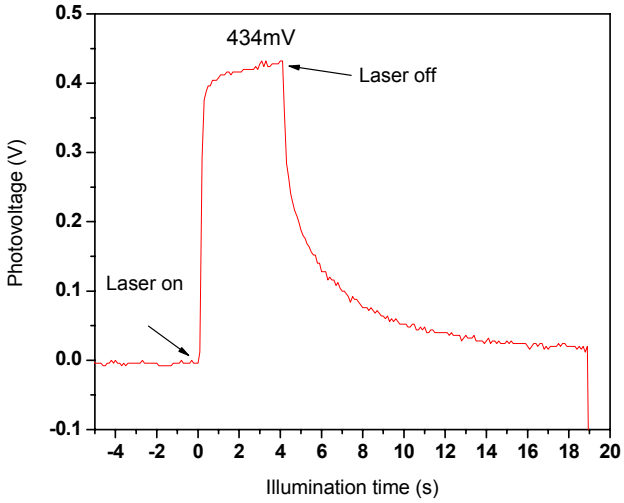

Figure 10. Photovoltage response of an InP QD PPD. The PPD was illuminated by a laser operating at a wavelength of 532 nm and an incident power of 245 mw applied for five seconds.

3.4 Tuning the Optical Absorption of InP QDs to the Near-IR

A second QD synthesis was performed by NS to tune the size of the InP QDs to form ~ 6 nm sizes in order to shift their optical absorption to the near- IR range and to develop efficient PPD response over a broad spectral range. An InP QD solution resulting in a dark gray appearance was prepared via the colloidal chemistry method using trimethyl indium $(CH_3)_3In$ and tris(trimethylsilyl) phosphine$[(CH_3)_3Si]_3P$ as the reactive agents. The method of preparation was similar to the preparation of the first series of InP and

CdSe QDs, but was prepared at a temperature greater than 300°C and, the reaction time was controlled for approximately one hour. A second modification in the preparation involved coordinating the as-synthesized InP QDs in TOPO and TOP on the QD surface in order to achieve monodispersion stability. The InP QDs were precipitated using methanol, and washed with large amounts of methanol to remove extra TOPO and TOP. Finally the QDs were dispersed in toluene for characterization and eventually for the fabrication of PPDs samples that would be used in irradiation experiments.

Figure 11 is a TEM image of the synthesized InP QDs that were later incorporated into In QD PPDs used in the gamma-ray and proton irradiation studies. The TEM image indicates that the size of the InP QDs predominantly ranged from 3 nm to 6nm. Also evident are small amounts of InP QDs with sizes ranging from >6.0 to 10 nm. The statistical ensemble results in an approximate average QD size of ~5-6 nm.

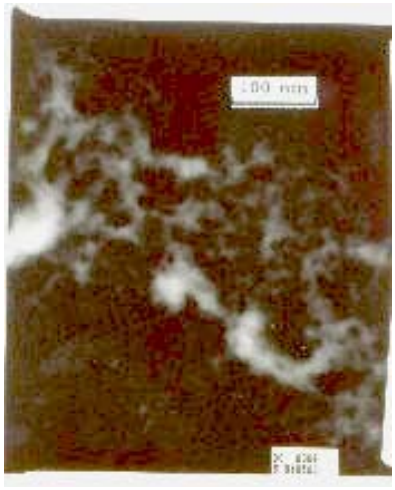

Figure 11. TEM image of InP QD sample #4. QDs ranging in size from ~3-10 nm are shown in comparison to the 100 nm calibration scale (insert).

The optical absorption from the ultra-violet (UV) to the near-IR for the InP QD in solution is shown in Figure 12. The absorption shown in Figure 12 is dominated by InP QDs with sizes less than 5nm, while small amounts of larger size QDs or aggregations of QDs larger than 6nm absorb in the near-IR range (~750 to 920nm) [4].

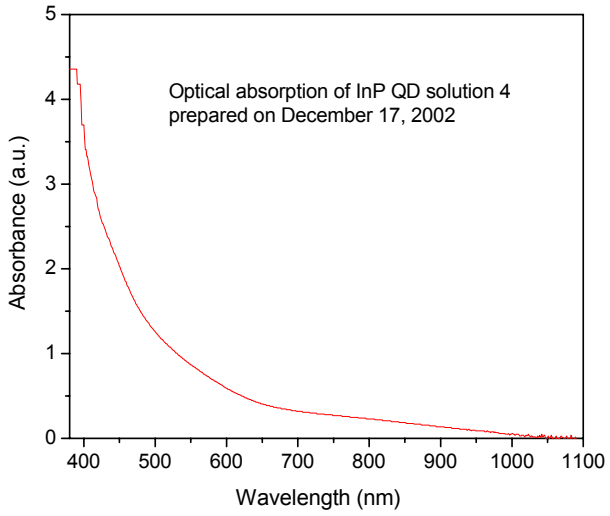

Figure 12 . UV to near-IR optical absorption of In QDs in solution.

All of the PPD samples for irradiation experiments consisted of InP QDs prepared from the second synthesis procedure. Figure 11 demonstrates that InP QD sizes predicted for absorbing in the near-IR range PPDs were incorporated into the PPDs. Figure 12 also indicates that while the QD absorption extended to $\lambda \sim 1000$ nm, the magnitude of the absorption was suppressed at near-IR wavelengths. However, sufficient absorption occurred in the near-IR allowing study of the radiation –induced effects over the entire InP QD PPD spectral response range (~ 400-1000 nm).

4.0 RADIATION INDUCED EFFECTS IN QD POLYMER-BASED PHOTODETECTORS

Polymer-based photonic (PBP) technology includes materials and devices such as electro-optic modulators, light emitting diodes, lasers, optical waveguides, detectors and other active and passive polymer components that comprise photonic systems. Recently, parallel studies for determining the radiation resistance of electro-optic polymer modulators have been enjoined by AFRL for understanding the underpinnings of the interaction of NLO polymers with ionizing radiation. Ongoing and previous irradiation

studies of PBP devices performed by IPC have examined the degree of radiation resistant exhibited by various linear and NLO polymer materials and NLO polymer modulator devices [10-15].

As recently reported, irradiating photovoltaic PPDs using gamma-ray and protons radiation early in material or device development stage provides an early quantitative measure of the PPD response to ionizing and nuclear particle induced displacement effects [1,2]. Quite often promising photonic materials and devices are developed at great expense and later found to be lacking in their ability to resist or survive in radiation environments. Empirical radiation response data is important for the early selection of radiation resistant materials and for eventually determining the underpinnings of the radiation-induced degradation processes in new and emerging polymer materials. An early and aggressive approach for determining the radiation resistance of materials and devices mitigates costly radiation effects studies and qualification testing of new technologies under space environment conditions. Space qualification testing on many components is too often performed at a later date on highly developed, widely applied, but not necessarily radiation resistant technologies. Often during space qualification parts-testing, heroic efforts are required to redesign non-hardened technology or to invoke costly and protective measures (i.e. using shielding materials) for new technologies "soft" to space radiation environments. The investigation of the relative radiation resistance of promising polymer materials for PPDs presented in this report are a first step to rectify this existing and all too-frequently repeated historical problem, by identifying and gaining an early understanding of the effects of ionizing radiation on emerging and state-of-the-art polymer detector materials and devices. QDs have been incorporated into inorganic polymer detectors with reasonable success in order to manipulate the detector spectral response. Inorganic QD infrared photodetectors (QDIPs) operating well into the mid infrared have attracted much attention due to the ability of varying the quantum well structure and dot size in order to change the photoluminescence spectra [16]. Enhanced radiation resistance in QD-doped InAs/GaAs lasers irradiated by various high energy ions have been reported showing that interaction of charge carriers with non-radiative defect centers are reduced due to efficient exciton localization by QDs [17-21].

4.1 Radiation Induced Effects in InP and CdSe QD PPDs

Recent radiation-effects data has been reported for several promising PBP materials used in polymer electro-optic modulator devices which suggest that other polymer photonic devices may soon be developed that will surpass a variety of inorganic-based photonic devices in performance parameters and in resistance to gamma-ray and energetic particles. However, little is known of the role that QDs will play in the hardening of polymer-based photovoltaic detectors. In the paragraphs that follow, empirical radiation effects data is presented based on InP and CdSe QD PPDs investigated by IPC and NS. The data provides a first step in determining whether InP and CdSe QD based photovoltaic detectors have potential for further development. The investigation of the effects of gamma-ray and proton irradiation on InP QDs doped PPD samples was accomplished using the Sandia National Laboratory (SNL) Gamma- Ray Irradiation Facility (GIF), in Albuquerque, NM, and the Crocker Nuclear Laboratory (CNL) isochronous cyclotron at the University of California, Davis, CA. CdSe QD PPD samples were also irradiated at the SNL GIF.

4.2 Gamma-Ray Irradiation of InP QD PPDs

Shown in Figure13 is the physical arrangement under which the gamma-ray irradiations of QD PPDs were conducted. PPDs and thermoluminescent detectors (TLDs) used

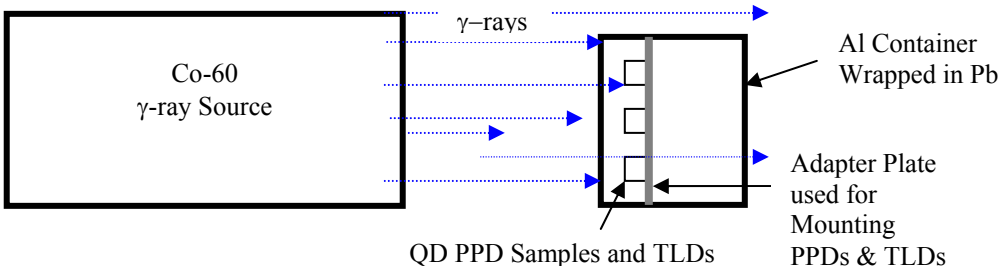

Figure 13. Arrangement for gamma-ray irradiation of InP QD PPD samples. A lead (Pb) wrapped aluminum (Al) container (Pb-Al) was used to reduce low energy photons and to shield the samples from ambient photo-degradation effects [22]. PPDs and TLDs for measuring the gamma-ray dose were located in proximity to each other. Gamma-ray (γ-ray) are shown by blue arrows.

for measuring the gamma-ray dose were mounted in proximity to each other on an acrylic adapter plate which positioned the samples normal to the gamma-ray source.

Figure 14 shows a typical InP QD PPD viewed from the counter-electrode side. As can be observed, the PPD consists of four active-isolated detector elements comprising an array. The individual detectors are shown separated by vacuum tape and coated by Al to form the counter-electrode shown in Figure 6. Photovoltage outputs from the four active areas comprising the array were averaged to represent the PPD photovoltage output.

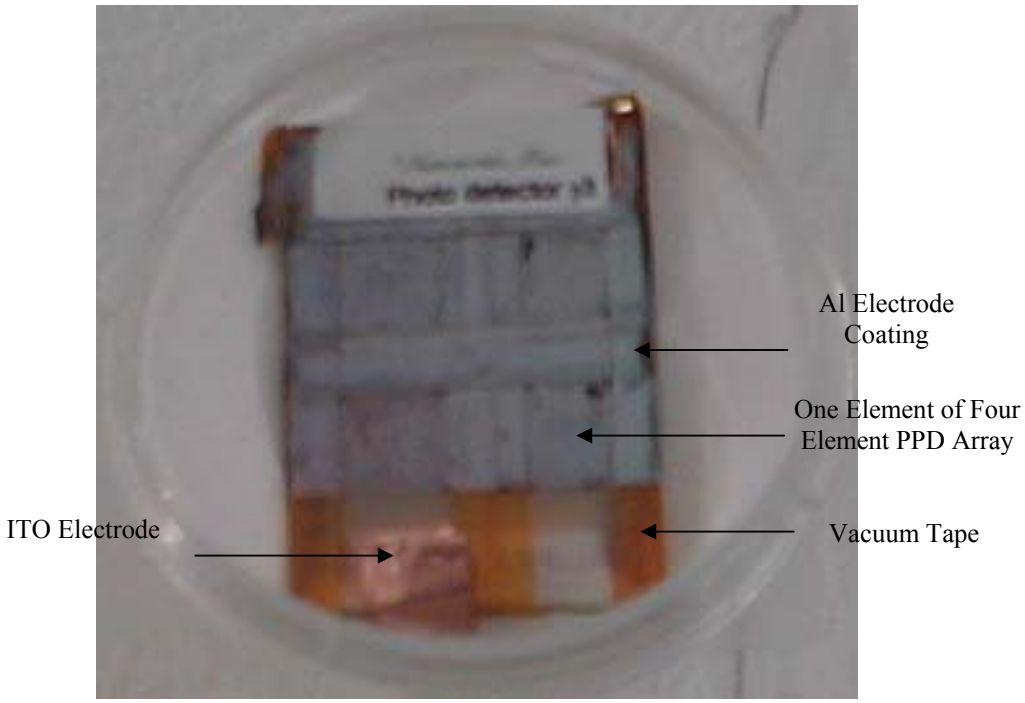

Figure 14. Photograph of a typical InP QD PPD array. The PPD sample is viewed from the top (Al counter-electrode side). The device is shown segmented into four isolated Al-coated detector areas that comprise the array. Vacuum tape helps to define the active areas.

Shown in Figure 15 is the arrangement of several Pb-Al containers situated perpendicular to the SNL gamma-ray source. The InP and CdSe QD PPDs were enclosed within the sealed Pb-Al containers during the irradiation and protected from room lighting which is known to contribute to aging effects in polymer detectors.

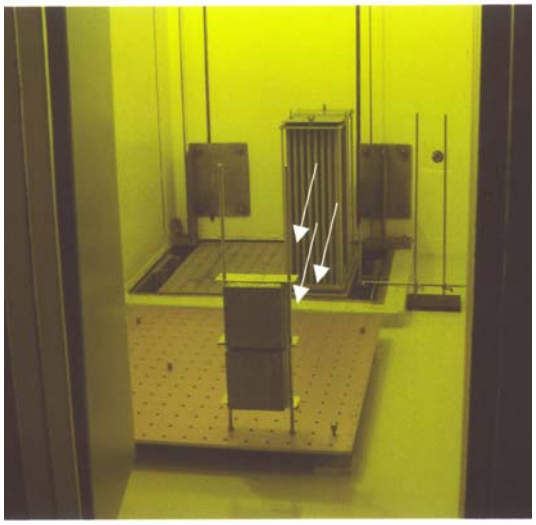

Figure 15. Irradiation of QD PPDs at the SNL GIF. Shown in the foreground are two stacked Pb-Al containers with PPD samples enclosed within the container volume. The gamma-ray source is shown elevated from its water storage/shielding area and can be seen in the background. Arrows from the source show the gamma-rays directed towards the Pb-Al container.

The SNL dosimetry was optimized using a Pb-Al container (also referred to as the irradiation volume) to attenuate the low energy photons since the presence of these photons in the incident spectrum can cause dosimetry errors. Use of the Pb-Al container shown in Figure 15 assured that lower energy photons (< 1 MeV) were greatly attenuated or absorbed in the Pb-Al container walls. Low energy photons are created by Compton scattering of the Co-60 gamma-rays within the source structure and or within materials that lay between the source and the irradiated device, as well as within materials that lie beyond the device but contribute to backscattering. The container also prevented unwanted exposure of the samples to sustained periods of room lighting which is known to induce "aging" via photo-degradation processes. The uncertainty in the SNL-GIF dosimetry measurements was ~<10%.

Prior to the onset of irradiation, gamma-ray dose and dose rate mapping was accomplished to ascertain dose rate variations and to identify the optimum spatial coordinates required for aligning the samples perpendicular to the gamma-ray source. Following each of four incremental irradiations, selected samples were removed from the

acrylic holder plate and placed in a protective storage container occupied by the control sample. Dosimetry considerations consisted of selecting the proper number and type of dosimeters for confidently measuring the irradiation dose, and locating the dosimeters in proximity to the samples. Multiple CaF_2 TLD arrays consisting of 4 TLDs per array measured the dose received by each sample. The array arrangement insured an accurate measurement of the gamma-ray dose received by each sample and provided multiple dose point readings for averaging the total dose across the target area. The irradiated TLD arrays were removed following each incremental irradiation and replaced by fresh TLDs in readiness for the next incremental irradiation.

The glow-curve readings of the TLDs and the dose and dose rate statistics were performed by the SNL Radiation Metrology Laboratory. The standard deviation in dose are SNL estimates based on random uncertainties in TLD responses at Co-60 energies and are reported at the 1-sigma level. At Co-60 energies, the Dose (Si) is calculated as Dose (Si) = Dose (CaF_2) x 1.02. Shown in Table 1 are the average total dose and and average dose rates for the entire sample set.

Table 1. Gamma-ray irradiation dosimetry.

Gamma-ray Irradiation [No.]	Dose [krad(Si)]	Dose Rate [krad(Si)]/min	Temperature [ºC ± 0.5]	Uncertainty (%)
1	8.9	107	18.1	7.3
2	45.2	102	18.9	7.8
3	96.3	100	18.9	13.8
4	151	102	18.6	14.0

4.3 InP QD PPD Pre- and Post-Gamma-Ray Irradiation Reponses

Table 2 lists the averaged pre-and post- irradiation photovoltages for the InP QD PPD samples, the dates measurements were performed and the gamma-ray dose for each irradiated sample at an average dose rate of 103 krad(Si)/min as shown in Table 1. Table 2 also includes the sample photovoltages measured over a six week aging study of the eight irradiated samples and one non-irradiated control sample.

Table 2. InP QD PPD pre- and post gamma-ray irradiation responses.

γ-Ray Dose [(krad(Si)]			8.8	9.0	44.4	45.9	94.3	98.2	150.7	152.1	Control Sample
InP QD PPD Sample			g_{11}	g_5	g_9	g_{10}	g_2	g_6	g_7	g_3	P_6
Date, Week, Test			*Photovoltage (PV) measured in mV								
1/13/03	0	Pre-Irrad.	462	307	464	614	439	488	553	442	495
1/27/03	2	Post-Irrad.-	459	296	370	543	258	298	342	178	311
Δ PV (decrease in PV)			***3***	***11***	***94***	***71***	***181***	***190***	***211***	***264***	***184***
2/04/03	3	Aging 1	321	248	333	467	272	254	328	236	253
2/11/03	4	Aging 2	289	249	337	457	242	226	362	190	175
2/18/03	5	Aging 3	233	215	281	379	212	231	313	188	162
2/25/03	6	Aging 4	262	169	286	316	249	274	264	225	160

*Note: Data shown were obtained at an incident laser power of 245 mW, at a wavelength of 532nm and with a beam waist diameter of 3mm. Averaged photvoltage responses were measured at four different active areas on each sample (on the same date). The uncertainty in the photovoltage measurement data is estimated at ~5% to 8%.

4.4 Analysis of Gamma-Ray Irradiated InP QD PPDs

As can be observed in Table 2, the samples were irradiated on January 20, 2003 and were measured for their post-irradiated photovoltage output responses on January 27, 2003. Aging studies were then conducted weekly for one month on the irradiated samples and on the non-irradiated control sample using facilities at the Fiber & Electro-Optics

Research Center (FEORC) at Virginia Tech. Photovoltage measurements were conducted using a laser system with an incident optical power of 245 mW and a nominal 3mm beam waist diameter incident at the sample surface (see Figure 9a).

In Figure 16 the post-irradiation data clearly indicates that the photovoltage responses for each PPD sample decreased following irradiation by gamma-rays.

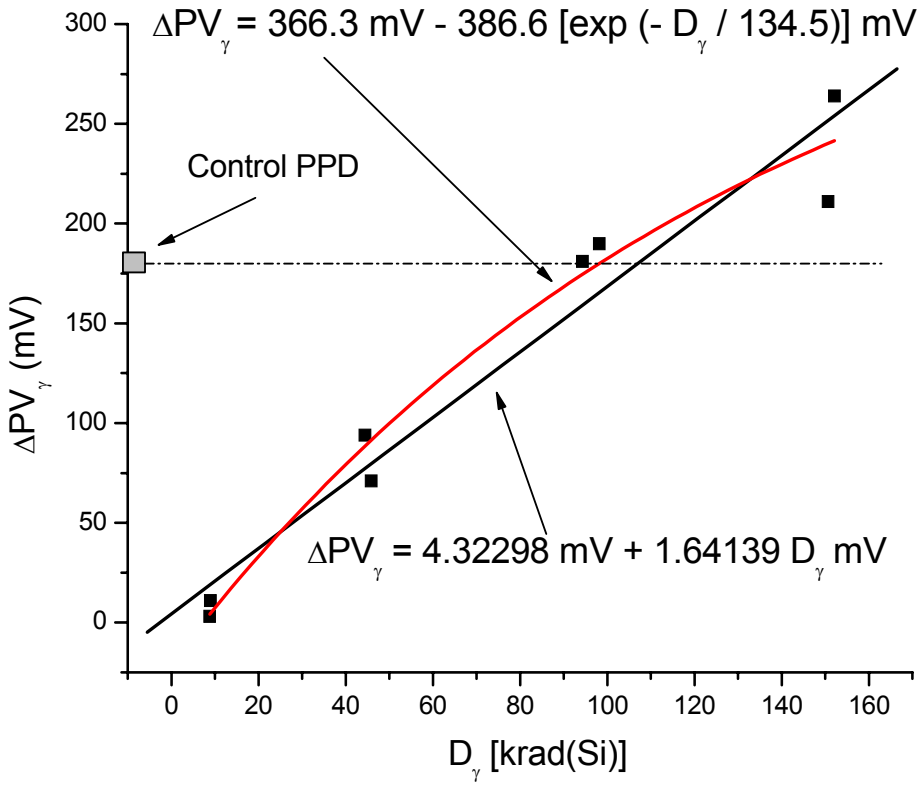

Figure 16. Reduction of InP QD PPD photovoltage following gamma-ray irradiation. Linear and first order exponential curve fits are represented by the black and red solid lines, respectively. The horizontal dashed line depicts the reduction (ΔPV) in photovoltage for the non-irradiated control PPD resulting from the natural aging process over the two week period between pre-and post- irradiation measurements (see Table 1). As can be seen, the photovoltage output response of the control PPD is greater than many of the irradiated PPDs. The control sample data is not part of the data used in the curve fitting.

The photovoltage response data includes combined gamma-ray induced losses in the PPDs contributed by: 1) the active QD-polymer matrix material, 2) ITO electrode and 3) the glass (borosilicate) substrate. Previous IPC and NS measurements of gamma-ray induced transmission loss through identical glass substrates at $\lambda \sim 532$ nm revealed that

the incident light intensity incident on the active detector area is reduced by approximately: 0.5 %, 2%, 4% and 6% at doses of ~10, 50, 100 and 150 krads(Si), respectively [23]. Thus, the light intensity reaching the PPD active area is reduced by radiation induced color centers in the glass substrate. Light intensity attributed to radiation darkening in the 200 μm thick ITO electrode was determined to be minimal at the applied doses [24].

In Figure 16, the expressions for the linear and exponential curve fits are given as:

$$\Delta PV_{\gamma} = V_L + 1.64\ D_{\gamma} \quad (1)$$

and

$$\Delta PV_{\gamma} = 366.3 - 386.6\ [\exp(-D_{\gamma} / 134.5)] \quad (2)$$

respectively.

In Equations (1) and (2), ΔPV_{γ} represents the curve-fitted decreases in photovoltage [i.e. (mV)] for an applied dose (D_{γ}) expressed in krad(Si). As can be seen in Eq. (1), $V_L \sim 4.32$ mV at $D_{\gamma} = 0$. Considering that the measurement of the photovoltage outputs were estimated to be 5-8 %, V_L falls well within the measurement uncertainty range. The linear fit provides information regarding the induced degradation rate ΔPV/[krad(Si)] for the applied dose range and can be obtained from Equation (1) as ~ 1.64 mV/[krad(Si)]. The linear fit provides an upper bound for estimating the potential gamma-ray induced decrease to the PPD photovoltage output with applied dose. Clearly, no indication of saturation for the induced photovoltage decrease is possible with the linear curve fit.

However, for samples g_7 and g_3 irradiated at doses of 150.7 and 152.1 krad(Si), respectively, the first–order exponential curve fit shown in Figure 16 and Equation. 2 appears to better accommodate the two PPD photovoltage responses at high dose and fits well with the remaining response data at lower dose. Examination of the exponential curve fit predicts a maximum decrease in photovoltage of ~ 366 mV at a proton dose of ~ 1 Mrad(Si) suggesting a potential for saturation of the induced degradation since the curve fit is highly asymptotic beyond this dose. Interpretation of the data would suggest

that this curve fit may provide an estimate of a lower bound to the photovoltage deterioration process resulting from the gamma-ray irradiation. The correlation coefficient for the exponential curve fit shown in Figure 16 is $R^2 = 0.96971$, indicting a good curve fit [25].

The non-irradiated control PPD (P_6) is also shown in Figure 13 but was not included in the data that were curve-fit. The control sample exhibited a decrease of 184 mV over the two week period that separated the PPD pre-and post– irradiation measurements. This large decrease in photovoltage output for the control device indicated the presence of a complicated deterioration process believed attributable to the environment (e.g. effects of moisture, oxidation, photosensitivity, temperature and other unknown factors that could affect the PPD photovoltage stability).

The photovoltage decrease in the non-irradiated control PPD shown in Figure 13 was attributed to "aging" and was nearly equivalent in magnitude (184 mV) to the photovoltage decreases observed for PPDs g_2 ($\Delta PV_\gamma = 181$ mV) and g_6 ($\Delta PV_\gamma = 190$ mV) which had been irradiated to doses of 94.3 and 98.2 krad(Si), respectively. The control PPD was kept in proximity to the pre- and post- irradiated devices except during the brief periods of gamma-ray irradiation where the control device was far removed from the devices under irradiation. Under these conditions, it is reasonable to assume that all devices experienced exposure to a common ambient environment. A further assumption made was that the non-irradiated control PPD was physically representative of the irradiated PPDs. Under this assumption it would not be unreasonable to expect that the Control PPD would experience less photovoltage degradation compared to the irradiated PPDs.

However, the data in Table 2 and Figure16 clearly show that three of the four irradiated PPDs pairs: [(g_{11}, g_5), (g_9, g_{10}), (g_2, g_6)] appear to have experienced less post-irradiation PV degradation than the non-irradiated control PPD. This data strongly suggests two possibilities: 1) that in some manner, the irradiated PPDs benefited from the γ- ray irradiation; 2) the control PPD aged at a rate faster than the irradiated PPDs or both

processes occurred. One possible explanation for the responses of the irradiated PPDs is that free carriers arising from the radiation process contributed to trap filling of native defects within the polymer composition. Trap filling is known to occur in crystalline and amorphous optical and electro- optical materials that possess numerous defects. If defects existed within the PPDs, or within the QDs, trap filling may have provided a mechanism for reduction in optical scattering and propagation losses as exhibited by the low dose irradiated PPDs. As shown in Figure 17, similar enhancement effects following irradiation have been reported for Ru- based polymer detectors and also in gamma-ray and proton irradiated non-linear polymer modulator devices [1,2].

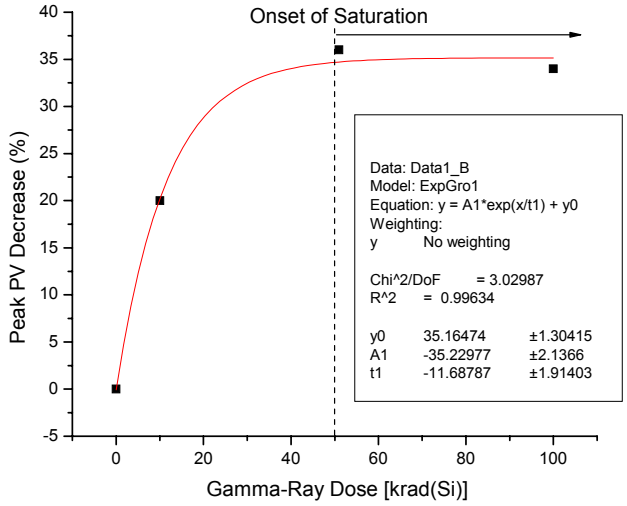

Table 3. Ru(N3) PPD gamma-ray irradiation data

Sample	Dose [rad(Si)]	Peak PV Decrease (%)
2	10	20
1A	51	36
1	100	34

Figure17. Photovoltage responses of N3 (Ru) Solid PPDs irradiated by gamma-rays. Insert in graph provides curve fit statistics [1, 2, 25].

Some polymer modulator devices have shown post-irradiation reductions in device scattering losses, insertion losses, propagation losses, extinction ratios and half-wave voltages [10]. Evidence of potential trap filling saturation effects in Ru(N3) PPDs was reported in a previous study conducted by IPC for AFRL/VSSS [1, 2].

In Figure 17 the data in Table 3 are fitted by an exponential growth curve. As can be seen, at low dose irradiations, the photovoltage loss increases at a rapid exponential rate as the dose increases to ~ 20 krad(Si). Past this dose, the theoretical curve fit turns over suggesting that the ionization-induced degradation at low dose is offset by other

competing processes, potentially trap filling of inherent defects within the polymer matrix. The theoretical curve fit suggests saturation of gamma-ray induced degradation at higher dose [>50krad(Si)] [1, 2].

Very little is known of the interaction of InP QDs irradiated by gamma-ray (~ 1.17 and 1.33 MeV) and high energy ions. The interaction of protons and gamma-ray with native defects, InP QDs, and the HTM material are also not known. Electron irradiations of n-type InP at ~≤ 2 Mev over 80-300K are known to introduce numerous defects below the conduction band which compete with native defects for free carrier removal [26]. Single crystal InP n^+-p junction solar cells with high substrate carrier concentrations show greater radiation resistance than either Si or GaAs single crystal solar cells [27-30]. Under gamma-irradiation, degradation of InP solar cells has been shown to result from: the reduction in carrier concentration in the p-InP substrate region (rather than in the active region); to increase the cell series resistance; and, a decrease in the minority carrier diffusion length with increasing photon fluence [27].

The data in Figure 17 further suggests that if trap filling via ionization– driven processes (i.e. ionization energies below dislocation energies) are occurring, the extent of trap filling by carriers may begin to diminish beyond a total dose > 100 krad(Si) as the number of intrinsic traps within the PPD become filled. Deep traps may continue to interact with inherent and ionization induced traps leading to a slow but diminishing growth in the trap filling process [26, 27]. Whether near- saturation (cessation) of the radiation-induced photovoltage degradation is realized (as suggested by Figure 17 for the Ru based PPDs) once filling of inherent traps is complete, cannot be determined unless studies of the irradiation and InP QD PPD interaction kinetics are performed at higher dose [i.e. >> 150 krad(Si)].

It may also be similarly argued from the data in Figure 16, that at low doses [$D\gamma \leq 100$ krad(Si)] and in comparison to the control sample photovoltage degradation, PPDs g_{11}, g_5, g_9, g_{10}, g_2 and g_6 did not experience significant ionization induced degradation to their respective photovoltages. This is also suggested by the near-equivalent photovoltage

responses of paired PPD samples irradiated to similar gamma-ray dose and the slow decrease of the photovoltage output at low dose. Data in Figure 16 and Table 2 also suggest that at the highest doses [~ 150.7 and 152.1 krad(Si) for PPD samples g_7 and g_3, respectively] that the samples (especially g_3) experienced considerable degradation in the HTM region which is evidenced by the diminished decay rate.

As will be shown in the next section, an aging study was conducted to ascertain the additional effects of the environment on all irradiated PPD as well as the non-irradiated control PPD. The aging studies also provide insight to potential annealing kinetics.

4.5 InP QD PPD Aging Studies and Results

Two aging studies of the PPD photovoltage output behavior over periods of months were performed following the post-irradiation measurements of gamma-ray irradiated PPD photovoltages and, the non-irradiated Control PPD photovoltage. The first of the aging studies was accomplished by measuring the photovoltage output response of all devices each week exposed to 5 second periods of illumination conducted over a period of one month using the 532 nm laser system represented earlier in Figure 9(a). Figures 18-22

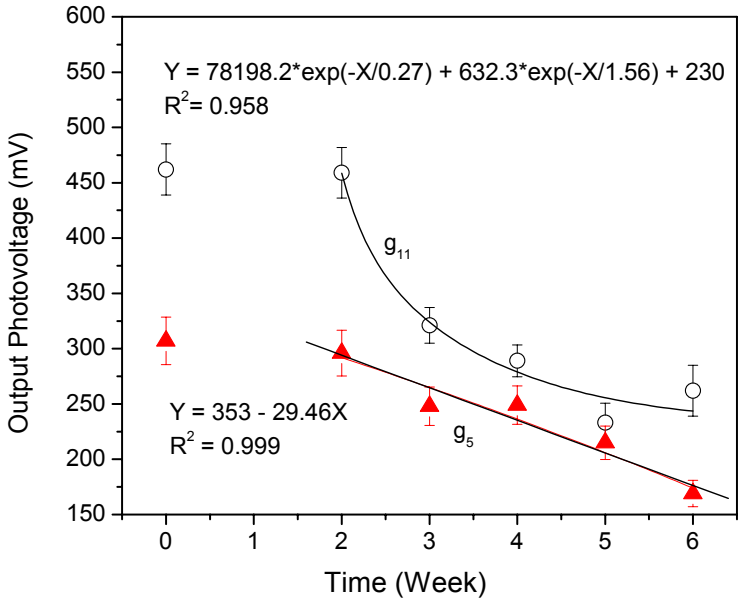

Figure 18. Aging of InP QD PPD samples g_{11} and g_5. Here, samples g_{11} and g_5 were irradiated at a dose of 8.8 and 9.0 krad(Si), respectively. Second order exponential and linear decay are evident for Weeks 2-6.

represent data for the observed aging (photovoltage decay) for the non-irradiated PPDs listed in Table 2. Samples exhibited widely ranging decay behavior including: first and second order exponential decay, as well as linear decay.

Where appropriate, equations expressing the linear and exponential curve fits in terms of the X-axis units [krad(Si)] and Y-axis units (mV) are shown in Figures 18-22 along with the correlation coefficient (R^2). In Figure 18, two off-set data points (circle and triangle) are shown at Time = 0 week and represent the pre-irradiation photovoltage measurement of PPDs g_{11} and g_5. The post- irradiation output photovoltages for g_{11} and g_5 were measured at Week 2 and the subsequent decay responses are shown for weeks 3-6. As can be observed, although these two devices were irradiated at nearly an identical dose [~ 8.9 krad(Si)] they exhibited different decay behavior indicating that the samples were not identical perhaps in composition, structure or were subject to different rates of oxidation due to inconsistencies in their preparation or packaging allowing interaction with the atmosphere. Figures 19-22 present similar data for the remaining irradiated PPDs.

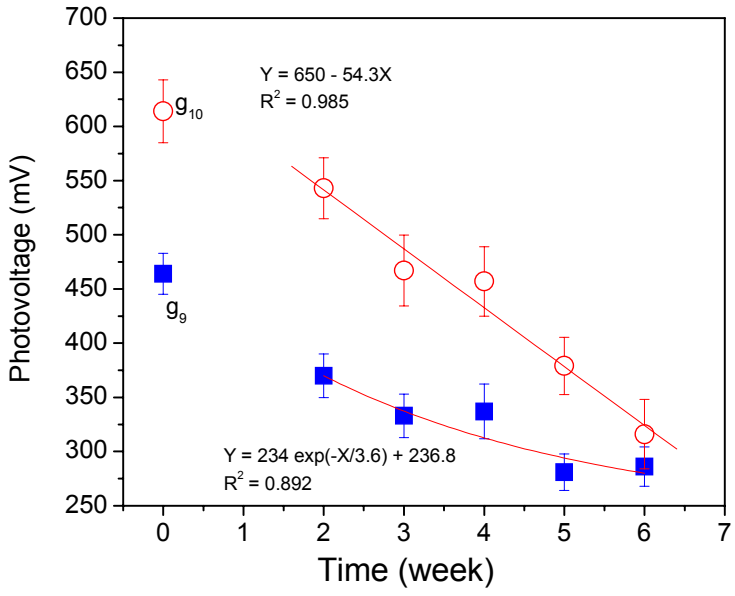

Figure 19. Aging of InP QD PPD samples g_{10} and g_9. Samples g_{10} and g_9 were irradiated at a dose of 45.9 and 44.4 krad(Si), respectively. Exponential and linear decay are evident for Weeks 2-6.

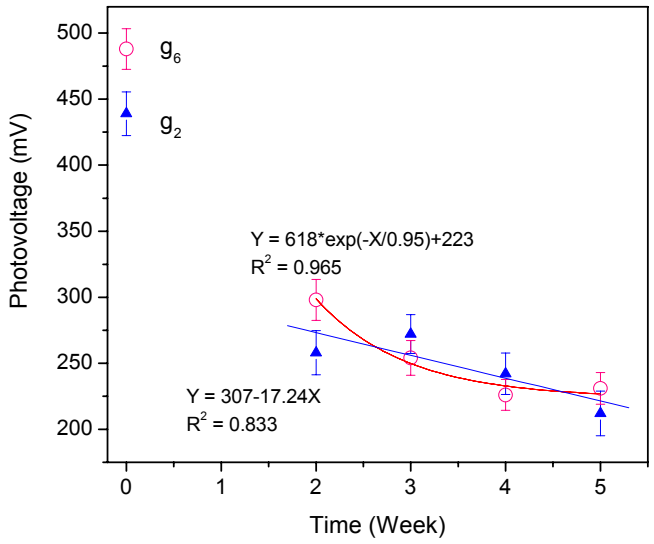

Figure 20. Aging of InP QD PPDs samples g_6 and g_2. Samples g_6 and g_2 were irradiated at a dose of 98.2 and 94.3 krad(Si), respectively. First order exponential and linear decay are evident for Weeks 2-5.

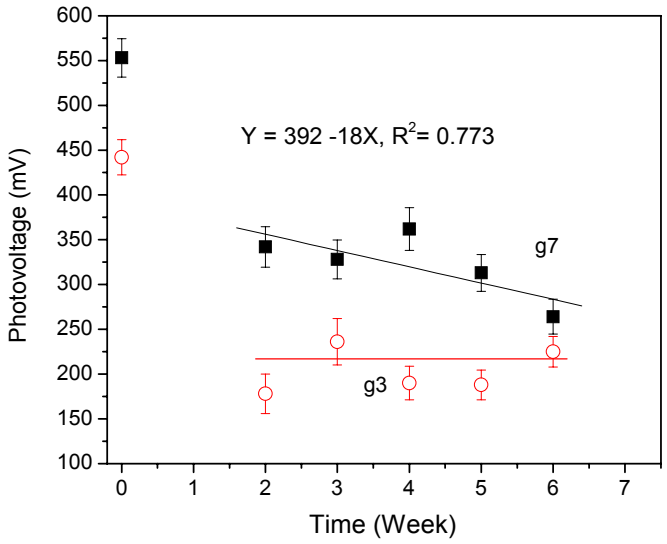

Figure 21. Aging of InP QD PPD samples g_7 and g_3. Samples g_7 and g_3 were irradiated at a dose of 150.7 and 152.1 krad(Si), respectively. Linear decay are evident for sample g_7 for Weeks 2-6, while it is believed that sample g3 exhibited substantial damage to the HTM polymer.

In Figure 21, samples g_7 and g_3 were irradiated to the highest doses and exhibited very small decays after the irradiation suggesting that the HTM polymer may have sustained

substantial damage. If so regeneration of the charge carriers would be impeded. The possibility that degradation to the TiO_2 and InP QDs materials also occurred cannot be dismissed. Based on other radiation effects studies performed on QDs, there is reported data to support the assertion that that the QDs were probably the least affected by the gamma-rays [17-21]. An independent study of the effects of radiation on these components would be required to differentiate the extent of degradation experience by each of the major components comprising the PPD.

Shown in Figure 22 is a representative example of the integrated natural aging of the InP QD-PPD Control device (P_6). The decay in the PPD output photovoltage results from the interaction of HTM, InP QD and TiO_2 with the environment of moisture and oxygen, as well as changes photo-chemically induced by ambient light and deliberate optical illumination during the evaluation and aging studies.

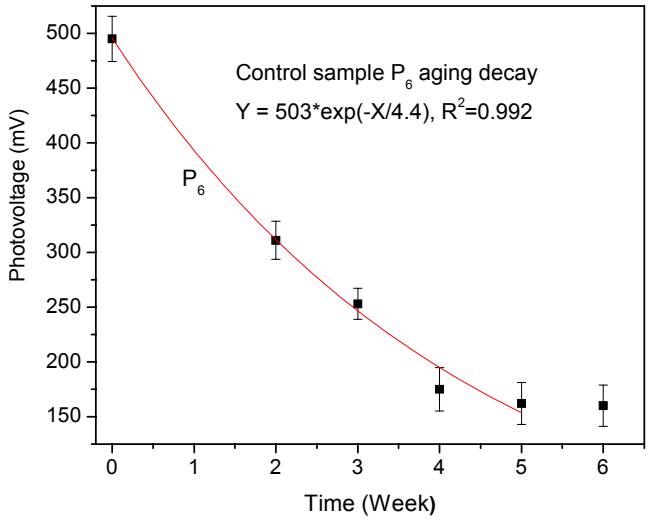

Figure 22. Natural aging of control sample P_6.

Examination of the PPDs photovoltage responses over a range of near- IR wavelengths was of special interest since the purpose of incorporating the InP QDs into the polymer PPD matrix was to ascertain the viability of using InP QD for shifting the PPD responses to longer wavelengths (i.e. $\lambda \sim 1000$ nm).

A tunable broadband solar simulator was used to illuminate the PPDs from approximately 400-1100 nm. Figure 23 represents the output power spectral density of the simulator source. Each sample was illuminated over an active area of 0.28 cm^2.

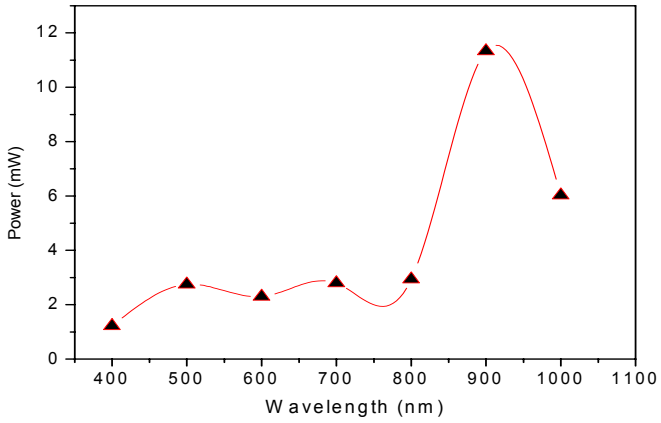

Figure 23. Power output of solar simulator source.

The PPD photovoltage responses as a function of the solar simulator illumination wavelength was obtained by determining the maximum average photovoltage response for a corresponding wavelength. Figures 24 to 36 present the response spectra of each gamma-ray irradiated sample and the control sample P_6, respectively, including aging data. All PPDs exhibit photovoltage responses over the spectral ranges spanning visible to near-IR wavelengths, although, each sample has a different response magnitude at different wavelengths. All PPDs showed a maximum photovoltage response for illumination at 500 nm since most of the InP QDs absorption occurs in the spectral range less than 600 nm, and, since the light intensity of the solar simulator is peaked at 500 nm relative to other wavelengths.

A small percentage of InP QDs having above average particle size ≥ 6 nm), are responsible for the 600-920 nm absorption [5, 8]. The response data shown in Figures 24-36 demonstrate a corresponding spectrum of the photovoltage responses of each InP-QD PPD within this range. The PPD detectors g_{11}, g_9, g_{10}, g_2 and g_6, and control sample P6 provided photovoltage output responses of ~20mV at an illumination wavelength of λ = 900 nm. As shown in Figures 33 and 34, samples g_7 and g_3 photovoltage responses [at D_γ = 150.7 and 152.1 krad(Si), respectively] over the range of 800 to 900 nm were

suppressed relative to PPDs irradiated at $D_\gamma \leq 98.2$ krad(Si). This would indicate that g_7 and g_3 PPDs experienced significant ionization induced damage.

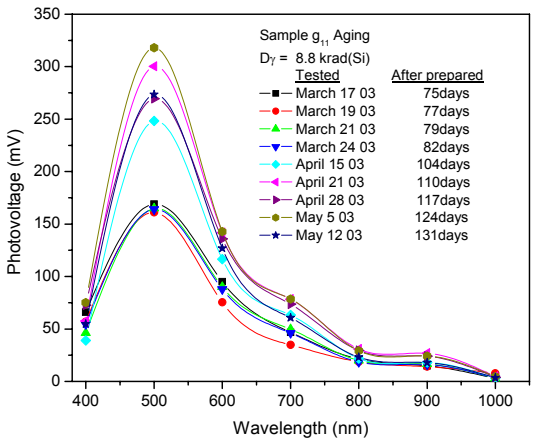

Figure 24. Aging of gamma-ray irradiated InP QD PPD g_{11}.

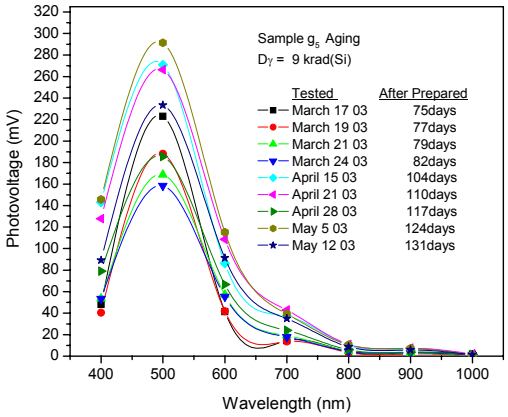

Figure 25. Aging of irradiated InP QD PPD g_5.

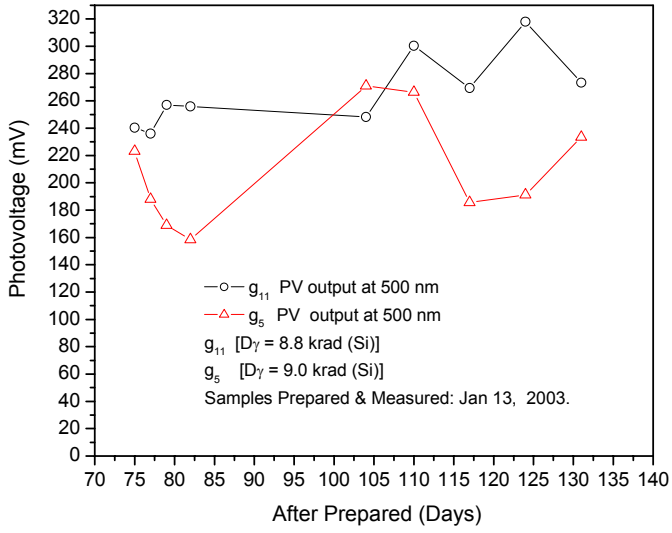

Figure 26. Aging comparison of gamma-ray irradiated g_{11} and g_5 InP QD PPDs.

It is important to recall that all samples were initially characterized for their photovoltage responses at $\lambda = 532$ nm on January 13, 2003 (Day1) and were irradiated on Days 7 and 8, while the measurements of the post-irradiation photovoltage were performed on Day 14 and next followed by the first series of laser-illumination aging studies spanning days 21-42.

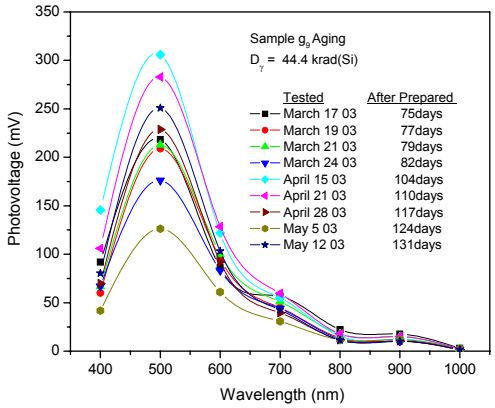

Figure 27. Aging of irradiated InP QD PPD g_9.

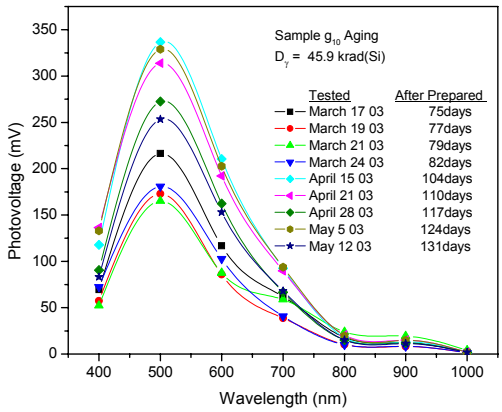

Figure 28. Aging of irradiated InP QD PPD g_{10}.

It is also important to note that the aging data shown in Figures 24-32 used a broadband light source rather than illumination by a laser centered at λ = 532 nm.. Thus, the period of time that lapsed between the first aging study and the broadband solar simulator aging study was some 31 days. The samples were stored in a dry, light free area during this period to prevent inadvertent environmental effects.

As can be observed in Figure 22, the second photovoltage aging study commenced on Day 75 after fabrication and characterization of the devices. In Figure 22, the complex aging behavior is displayed for the two InP QD PPDs, previously irradiated by low-dose gamma-rays. The measurements were performed at a wavelength of λ = 500nm and an illumination time of 5 minutes. A gradual recovery of the photovoltage occurred such that at the end of the aging study an increase in photovoltage was observed for all InP QD PPDs. These aging data are illustrated in Figures 24-32.

Depending on the regional combinations of electrons, holes and clusters of electrons and holes, various light-absorption bands can arise, which can combine to degrade the transmission and conductive properties of the material. The rate at which defects are formed (and annealed) can be influenced by impurities or even by inherent defects within the grown material as well as external factors such as temperature and photo bleaching.

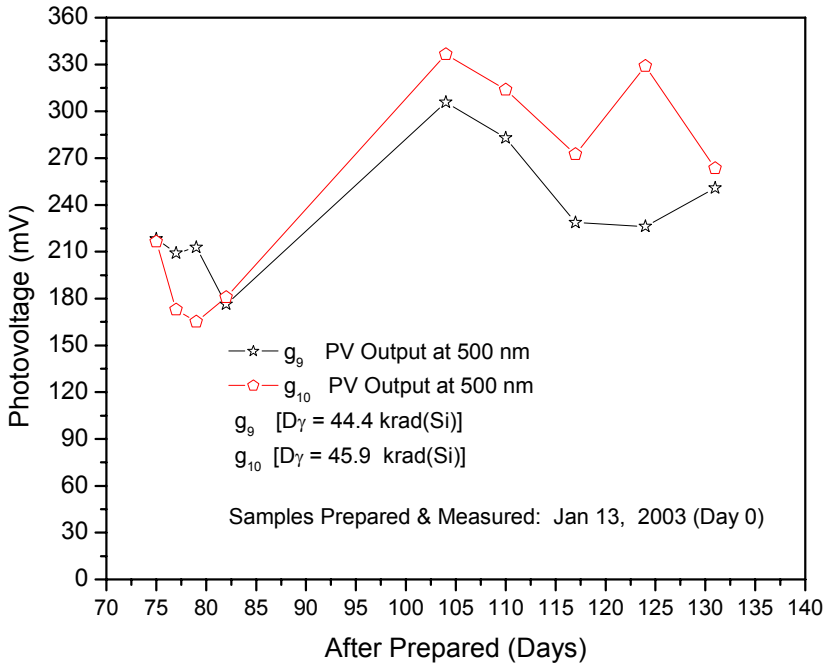

Figure 29. Aging comparison of gamma-ray irradiated g_9 and g_{10} InP QD PPDs.

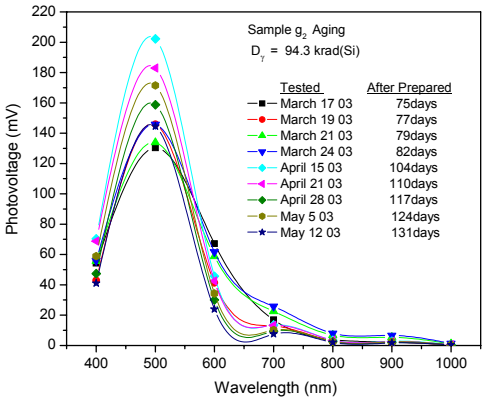

Figure 30. Aging of gamma-ray irradiated InP QD PPD g_2.

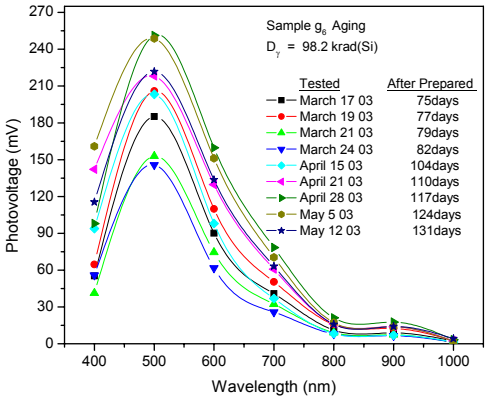

Figure 31. Aging of gamma-ray irradiated InP QD PPD g_6.

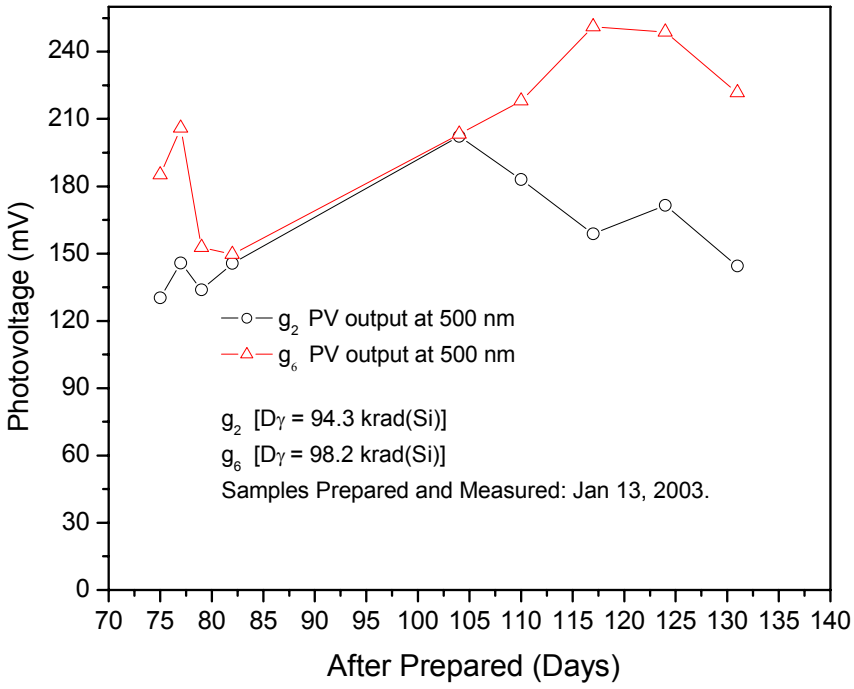

Figure 32. Aging comparison of γ-ray irradiated g_2 and g_6 InP QD PPDs.

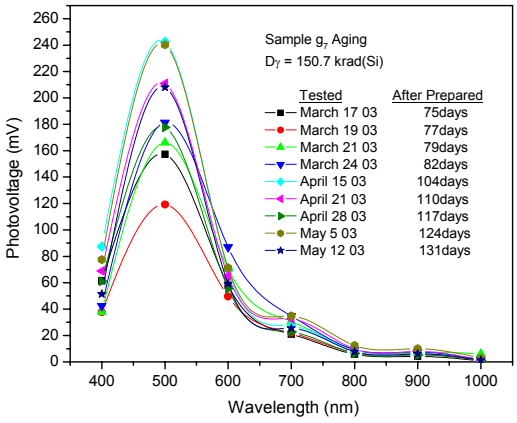

Figure 33. Aging of γ-ray irradiated InP QD PPD g_7.

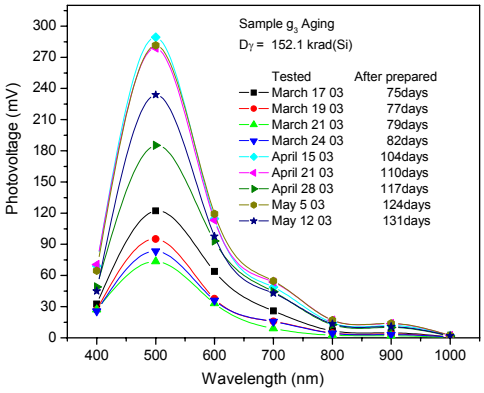

Figure 34. Aging of γ-ray irradiated InP QD PPD g_3.

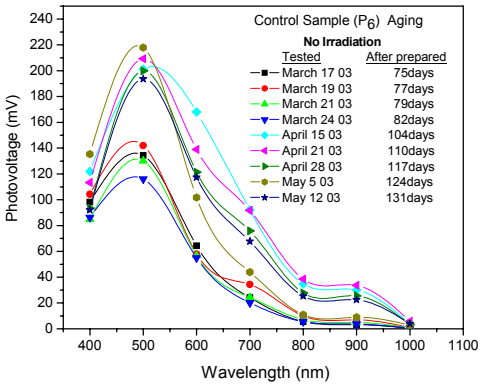

Figure 35. Aging of non-irradiated InP QD PPD control P_6.

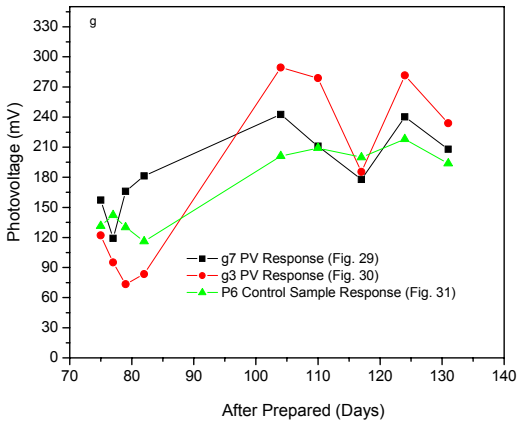

Figure 36. Aging comparison of samples g_7, g_3 and control P_6.

The three week aging study using a broadband optical source to illuminate the PPDs conclusively demonstrated that all InP QD PPDs including the Control sample PPD showed increases to their photovoltages by the end of the aging study (i.e. 131st day of the aging measurements). Table 3 compares the post-irradiation measurements (conducted on Day 21) with the end of the laser aging study and the end of the broadband illumination study (at Day 131).

Table 4. Comparison of InP QD PPD photovoltage during aging studies.

Sample	Day 0	Day 14	Day 21*	Day 42*	Day 75**	Day 131**
	InP QD PPD Photovoltage [mV]					
g_{11}	462	459	321	262	240	273
g_5	307	296	248	169	223	234
g_9	464	370	333	286	131	251
g_{10}	614	543	467	316	217	263
g_2	439	258	272	249	130	145
g_6	488	298	254	274	185	222
g_7	553	342	328	264	157	208
g_3	442	178	236	225	122	234
Control P_6	495	311	253	160	131	194

*Illuminated by 532 nm laser.
** Illuminated by broadband solar simulator source.

As can be observed in Table 4, all PPDs including the Control PPD decreased in PV output over time until broadband spectral measurements were commenced on Day 75.

The final measurements using the broadband solar spectrum source were conducted on Day 131 and conclusively showed that all PPDs experienced an increase in their photovoltage outputs relative to the measured photovoltage on Day 75. Since the measurements were made at room temperatures, the data suggests that photobleaching by the solar simulator was primarily responsible for the recovery of the photovoltage signal. Broadband illumination of the PPDs during the aging measurements may have caused photochemical and photo-physical changes to the device active components resulting in regeneration of the materials responsible for charge excitation (i.e. InP QDs) and charge regeneration and transport (HTM and TiO_2 materials).

The gradual increase in photovoltage with time suggests that the interaction between different components within the nanoparticle films, and especially at the Schottky barriers might be re-formed following illumination. These interactions would occur at the interfaces between TiO_2 and InP nanocrystalline particles, and InP QD and within the HTM regions.

It is clear that a complicated regeneration mechanism was responsible for the photovoltage aging behavior following the gamma-ray irradiation of PPDs and subsequent illumination by a broadband light source. Resolution of these interesting and important effects were beyond the scope and time limit allotted for this investigation, but should be actively pursued. A better understanding of the recovery mechanism may lead to developing improved radiation resistant PPDs.

4.6 Proton Irradiation of InP QD PPDs

Energetic ion irradiations are important for investigating and simulating long-term displacement damage in photonic devices that can and do occur in the natural space environment.

Degradation processes induced by energetic ions have not yet been extensively studied in polymer photodetectors. Ion-irradiations (e.g. protons and other ion particles such as Fe+, Ar^{+}, Ni^{+}) at high fluence can also induce large conductivity changes (i.e. increases to the material conductivity) and cause signal propagation losses in materials such as polyimide, polyethylene and other polymers which are used in various polymer-based photonic devices.

These and other material properties are especially affected during the time-frame the material is being exposed to the radiation flux. For example, the creation of transient conductive species and holes are formed during the time-period of the irradiation, but for the most part these species quickly recombine once the irradiation has ceased. During the irradiation, materials and devices may exhibit transient or brief degradation processes far in excess than are evident in post-irradiation measurements. For this reason, *in-situ* irradiations are critical in acquiring time-resolved device responses under dynamic irradiation conditions.

As a first step in understanding the effects of energetic ions induced in polymer detectors, *passive* rather than *in-situ* proton irradiation of InP QD PPDs were performed and are reported herein. As in the previously described passive gamma-ray irradiation studies, the proton irradiations also focus on long term radiation-induced effects which in all likelihood are diminished in magnitude compared to those occurring during *in situ* measurements. However, residual long–lived effects are often a good indicator that significant transient effects may be present. Compared to the results of the InP QD PPDs irradiated (under passive conditions) by gamma-rays, the proton-induced degradation effects will be shown to be much more pronounced and damaging to the output photovoltage responses.

Shown in Figure 37 is a block diagram of the equipment arrangement used by IPC to irradiate the InP QD PPDs by energetic protons, while Figure 38 shows the CNL isochronous cyclotron beam-line-output port used in irradiating the InP QD PPDs.

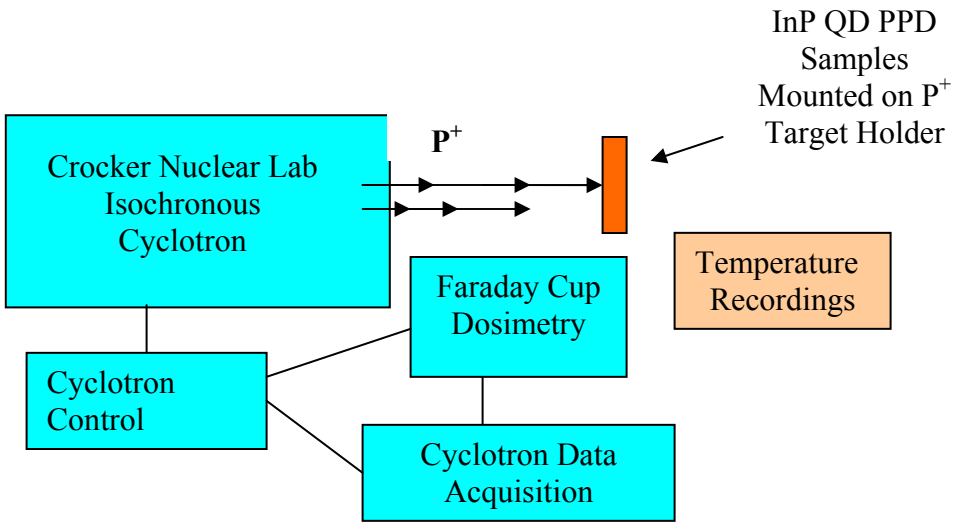

Figure 37. Equipment arrangement for proton irradiation of InP QD PPDs.

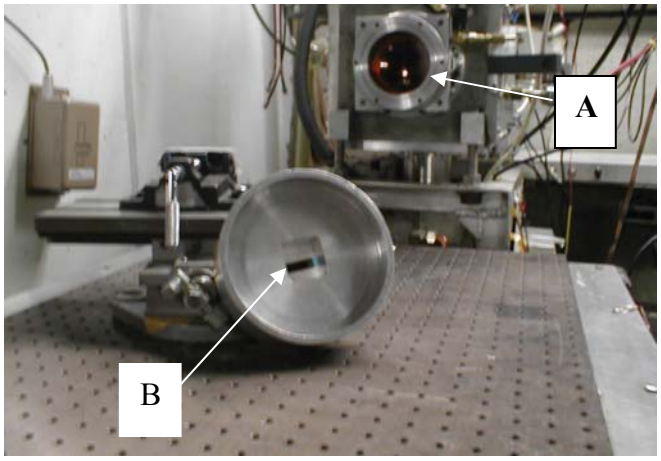

Figure 38. CNL isochronous cyclotron. **A)** Cyclotron output window, **(B)** Target holder used to position PPDs in the proton beam.

The appropriate proton energy was determined to be 25.6 MeV using SRIM modeling to insure that the protons completely traversed the PPD thin film claddings, glass substrate and electrode materials [31]. Dosimetery was accomplished using an in-line Faraday cup, and all irradiations were performed at room temperature T = 24 ºC (± 2.5 ºC). Typical beam size diameter over the PPD surface was ~ 2.0 cm with an average fluence of ~ 5 x

10^{11} p^+/cm^2. Measurements of the post -irradiation induced effects of 25.6 MeV protons at an average fluence of ~ 5 x 10^{11} p^+/cm^2 on the In QD PPDs were accomplished by Nanosonic using the FEORC facilities at Virginia Technical. The InP QD PPD output photovoltages were obtained under the same measurement procedures described earlier using a 532 nm laser operating at a power of 245mW with a beam spot diameter of 3mm applied for 5 seconds. Shown in Table 5 are the pre- and post-irradiation PPD photovoltage responses performed at room temperature. The uncertainty in the photovoltage measurements ranged from 5%- 8%.

Table 5. InP QD PPD photovoltage responses following proton irradiation.

Sample	Irradiation D_{p+} [krad(Si)]	Pre-Irradiation Photovoltage [mV]	Post-Irrdiation Photovoltage [mV]	Decreased Photovoltage* [mV]
P_1	10.1	617	597	20
P_2	49.9	442	407	35
P_4	99.6	388	345	43
P_5	99.7	521	424	97
P_7	150	529	201	328
P_{10}	150	596	348	254
P_{11} Control	N/A	377	337	40

*Note: Data shown were obtained at an incident laser power of 245 mW, operating at a wavelength of 532 nm and with a beam waist diameter of 3 mm. Averaged photovoltage responses were measured at four different areas on each sample (on the same date). The uncertainty in the photovoltage data is estimated to be ~5% to 8%.

As shown in Table 5, the photovoltage output of the InP QD PPD control device decreased by 40 mV from its initial pre-irradiation measurement of 377 mV, indicating it underwent modest aging (~10.6%) over the three month time period between pre- and post- irradiation measurements. This modest decrease in photovoltage (compared to the 184 mV photovoltage decrease observed for the InP QD PPDs control device used in the gamma-ray irradiations) suggested that the set of InP QD PPDs provided for the proton irradiations were quite stable, or, at least the control device was quite stable.

Table 5 shows a dramatic decrease in photovoltage for PPDs irradiated at high dose levels [$D_{p+} \geq 99.7$ krad(Si)]. Shown in Figure 39 is the graphical representation of the first order exponential decrease in the InP QD PPD photovoltage responses as a result of proton irradiations over the dose range of 10.1 - 150 krad(Si). The curve fit includes the control device data in the data set used to plot the curve. The photovoltage response for low dose suggests that a modicum of trap-filling may be occurring.

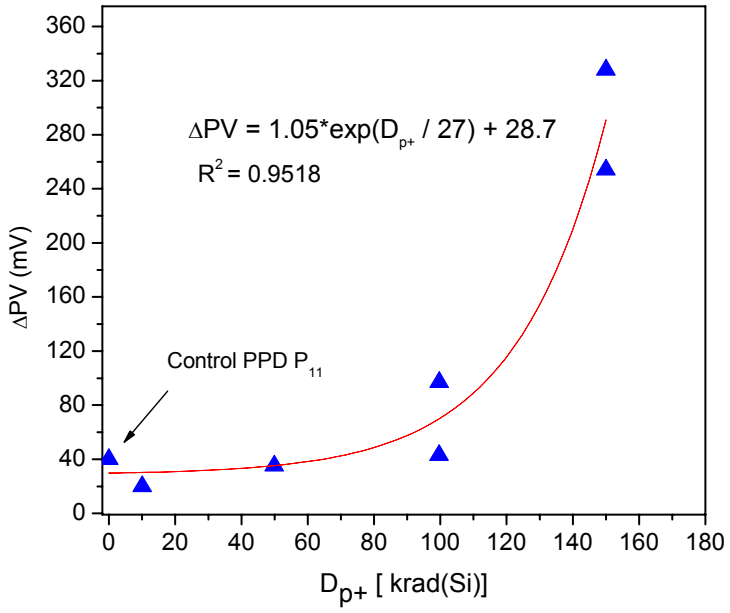

Figure 39. Proton-induced decrease in InP QD PPD photovoltage. Shown is the exponential growth in the decrease in photovoltage (ΔPV) for increasing proton dose (D_{p+}). The measurements were performed at a laser wavelength of λ = 532 nm, beam waist of 3mm and power output of 245 mW.

For $D_{p+} \leq 99.6$ krad(Si), samples P_1 and P_2 exhibited decreases in their photovoltage outputs less than that of the non-irradiated control sample, while the photovoltage of sample P_4 [irradiated to $D_{p+} = 99.6$ krad(Si)] agreed within 3 volts of the natural photovoltage decay observed for the non-irradiated control PPD. For $D_{p+} \geq 99.7$ krad(Si), PPDs P_5, P_7 and P_{10} exhibited significant decreases to their output photovoltages (97, 328 and 254 mV, respectively).

4.7 Aging Study of Proton Irradiated PPDs

The solar simulator described earlier in Figure 9(b) was used to investigate the PPD photovoltage responses at different optical wavelengths and to examine the aging behavior of the proton irradiated PPDs. Every PPD was illuminated over an active area of 0.28 cm^2 on the PPD surface. Figure 40 represents a typical photovoltage response of PPD P_7 to different wavelengths and intensities provided by solar simulator. Shown in Figure 40 is the response of sample P_7 three months after it was fabricated and irradiated by protons to a total dose of 150krad(Si). The near-IR peak responses at λ =900 and 1000 nm were 19.68 and 8.93 mV, respectively. As can be seen in Figure 40 the illumination intensity applied to the PPD varied widely due to the spectrum of the broadband solar source.

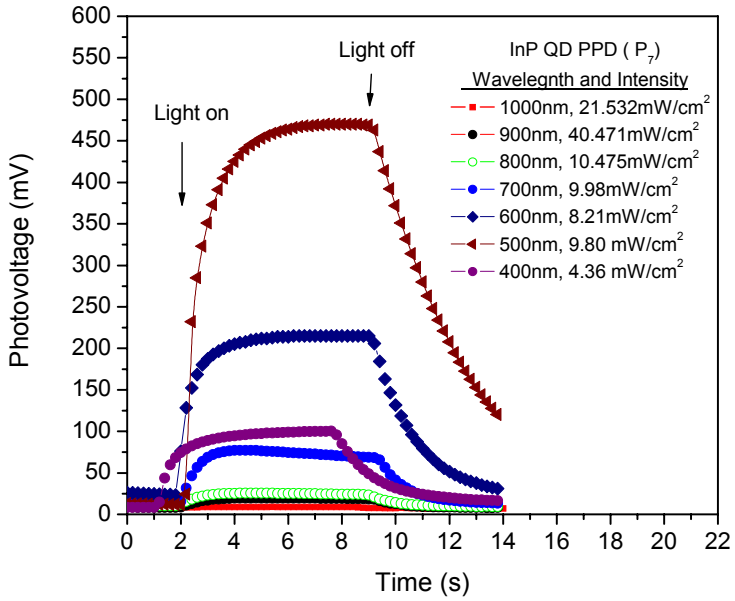

Figure 40. Visible to near-IR photovoltage responses for InP QD PPD device P_7. Responses following the proton irradiation of the device to a dose of 150 krad(Si) are shown.

The InP QDs prepared by NanoSonic exhibited absorption in the range of 380- 920 nm due to the wide variation in particle size. As shown in Figure 41, there is a very apparent decrease in the photovoltage output at λ = 532 nm after high dose proton irradiation.

However, as can been seen in Figure 40, the InP QD PPD P_7 demonstrated a wide spectral response ranging from 400nm to the NIR range (>900nm).

Caution must be used in comparing the response curves shown in Figure 39 and 40. In comparison to the solar simulator measurements, since measurements obtained with the laser system were conducted at higher optical power and illuminated smaller PPD surface areas. The laser illumination procedure may have potentially caused a significant portion of the incident light to not contribute to the output photovoltage. These and other issues such as repeatability in illuminating small active areas of the PPDs surface and non-uniformity in the detector surfaces due to the varying QD sizes and the distribution of the QDs could introduce errors.

Figure 41 presents the spectrally-resolved post-irradiation InP QD PPD photovoltage output responses under illumination by the broadband solar simulator. The non-irradiated Control sample P_{11} exhibited the highest output photovoltage signal at 500 nm, while the lowest photovoltage response at 500 nm was sample P_{10} irradiated to a total dose of D_{p+} = 150 krad(Si).

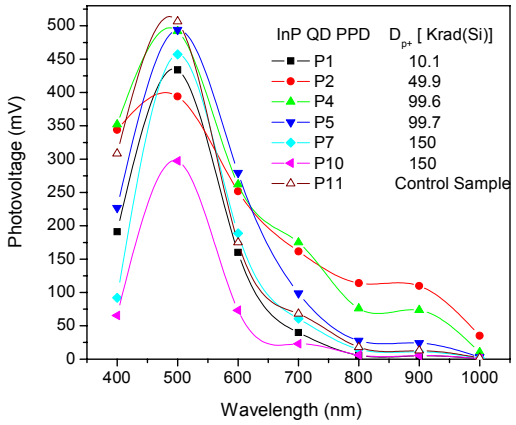

Figure 41. PV response spectra of all proton irradiated PPDs.

An aging study of the proton irradiated InP QD PPDs was also conducted using the broadband solar simulator as the light source. As can be seen in Figure 32 to 48, the aging curves depict the PPD photovoltage output as a function of time. In general the photovoltage decreases over time and the data also suggests that the aging process is

accelerated with increasing dose differing from the response of the gamma-irradiated PPDs data shown in Figures 24-36. The aging-time dependency is plotted in Figures 42-48 over wavelengths ranging from 400-1000nm in 100 nm increments. The PV response at each wavelength is plotted against time expressed in "Days after prepared'. Here, "Days after prepared" again represents the lapsed time between preparation of the sample (and its pre- irradiation measurement) and the particular Day that the broad band solar simulator measurement was performed.

The aging rate of the Control PPD (P_{11}, Figure 48) was less than the majority of irradiated PPDs, suggesting that the proton irradiation played a role in devices exhibiting accelerated aging rates. As shown in Figures 42- 49, the proton irradiated PPDs did not exhibit the extent of post-irradiation recovery as was observed during the gamma-ray aging studies. This is not an unexpected result, since the proton induced damage at equivalent dose is greater due to dislocations in the borosilicate glass substrate and in the components of the detector active area. Somewhat consistent with the recovery of the photovoltage output exhibited for the non-irradiated control sample (P_6) used in the gamma-ray studies, minimal aging or slight increases were observed in the photovoltage output for the control (P_{11}) device for 600 nm $\leq \lambda \leq$1000 nm.

As shown in Figure 49, the "flatness" of the aging curves at wavelengths 800nm, 900nm, and 1000 nm indicate that photovoltage decay is less pronounced at longer wavelengths. The data suggests that long-lived or permanent color centers caused by dislocations from the proton irradiations occurred and that photobleaching did not noticeably assist in recovery of the photovoltage. The data suggests that the damage or interaction mechanism of protons in the PPD was not the same as was observed for the gamma ray irradiations.

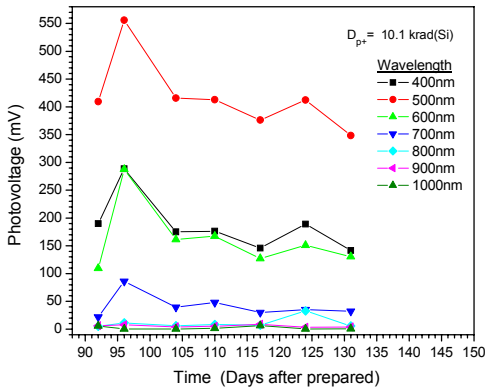

Figure 42. Aging behavior of InP QD PPD (P_1).

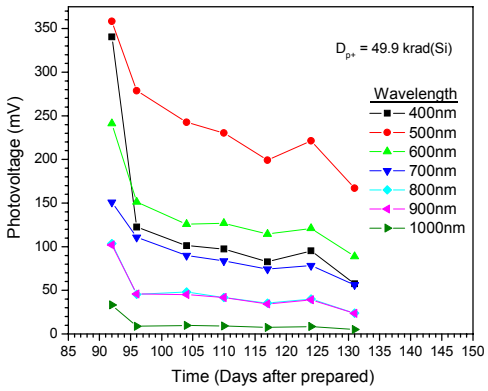

Figure 43. Aging behavior of InP QD PPD (P_2).

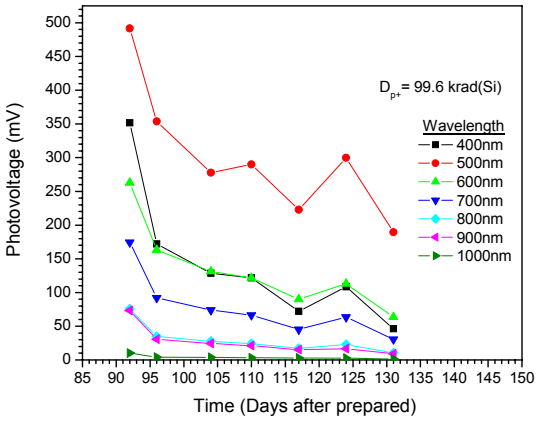

Figure 44. Aging of InP QD PPD (P_4).

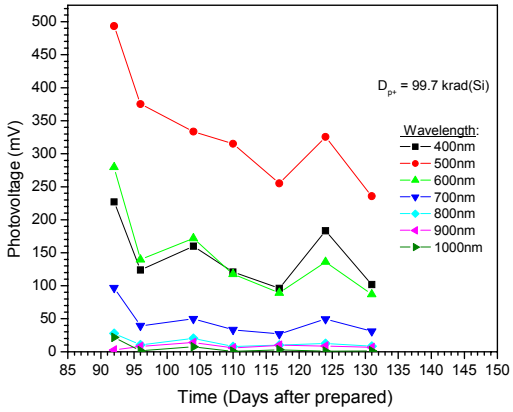

Figure 45. Aging of InP QD PPD (P_5).

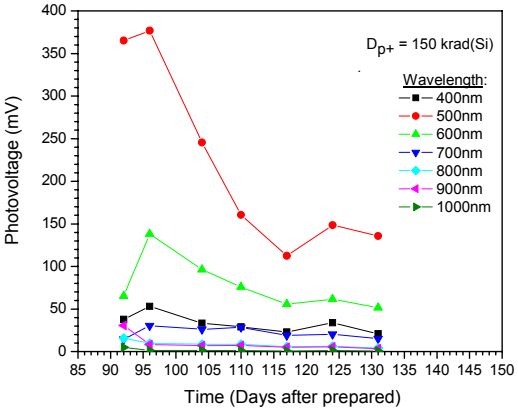

Figure 46. Aging of InP QD PPD (P_{10}).

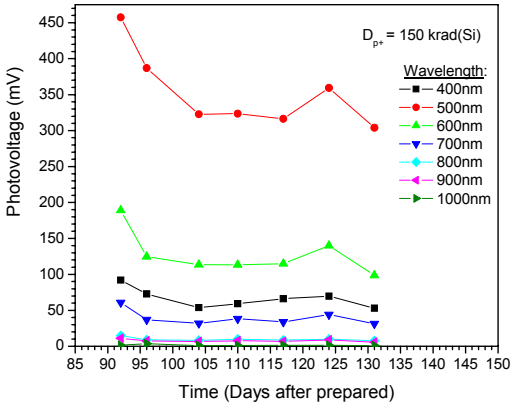

Figure 47. Aging of InP QD PPD (P_7).

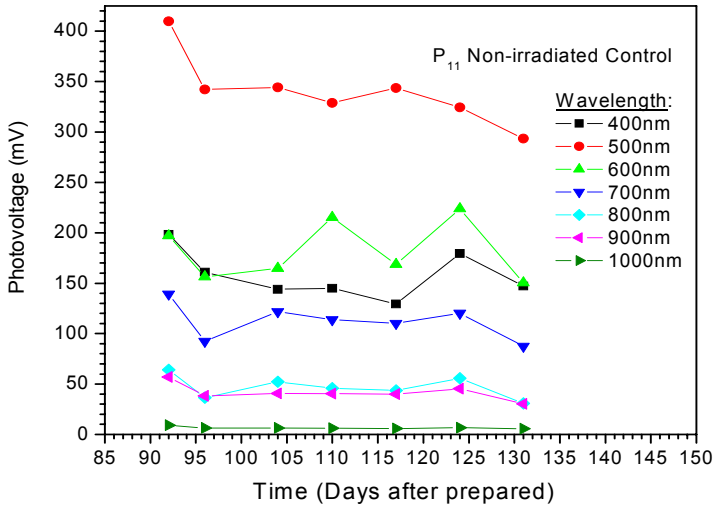

Figure 48. Aging of InP QD PPD Control P_{11}.

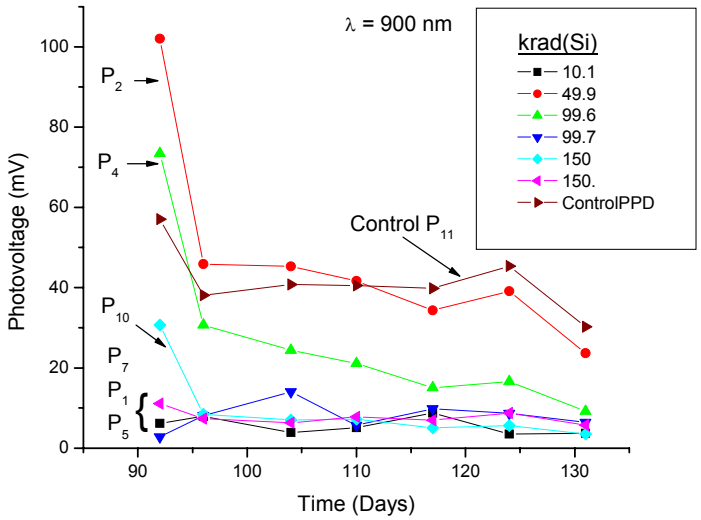

Figure 49. Aging response of proton irradiated InP QD PPDs at λ = 900 nm. As can be observed, aging is accelerated for $D_{p+} \geq 49.9$ krad(Si) as evidenced by the responses of PPD devices P_2, P_4 and P_{10}. PPDs P_7, P_1 and P_5 were severely degraded by the proton irradiations and do not appear to be displaying accelerated aging effects since their photovoltage outputs are greatly suppressed. A solar simulator was used as the illuminating source for the measurements.

Figure 49 is of special interest since the data represents the aging behavior of all proton – irradiated InP QD PPDs at a wavelength of λ = 900 nm [near the band gap of bulk InP

(i.e. λ = 918 nm)]. As may be observed only devices P_2, P_4, P_{10} and the control device P_{11} have sufficient signal remaining at Day 91 for undergoing additional decay of their photovoltages over the period Day 91- 131. The control device photovoltage decays but at a slower rate than do the photovoltages of P_2, P_4, P_{10} which were irradiated at 49.9, 99.6 and 150 krad(Si), respectively. The photovoltage outputs of PPDs P_7, P_1 and P_5 [irradiated at 150, 10.1 and 99.7 krad(Si)] are suppressed compared to the other PPDs, suggesting that these three devices were much more degraded by the proton irradiations and rapidly decayed to minimal output photovoltages. The variation in aging responses between the six irradiated devices and the control device further suggests the possibilities of: 1) wide variances in device chemical compositions; 2) variances in the spatial distribution, size and number density of the InP QDs within each device; and 3) the packaging of the devices were not uniform thus allowing inadvertent exposure of the samples to the environment. One or more of these factors could certainly change the dynamics of the PPD response data and resulting in the behavior shown in Figure 49.

As an example consider device P_1 shown in Figure 43, which exhibited the highest pre-irradiation photovoltage output (617 mV at λ = 532 nm) and received the lowest proton dose [10.1 krad(Si)]. The device exhibited a greatly suppressed photovoltage output at λ = 900 nm compared to devices P_2, P_4, and P_{10} which were irradiated at proton doses $\geq$ 49.9 krad(Si). P_{10} [irradiated to 150 krad(Si)] had a pre-irradiation photovoltage output of 596 mV (at λ = 532 nm) and continued to exhibit higher photovoltage output than P_1. Similarly P_2 and P_4 also outperformed P_1 at λ = 900 nm, as shown in Figure 49.

It is not unreasonable to attribute the observed post-irradiation response variances in the irradiated PPDs in part due to proton-induced effects. This assertion is evidenced by examining the aging behavior of the non-irradiated control device P_{11} shown in Figure 43. Despite having the lowest photovoltage output (377 mV at λ = 532 nm) among the samples, P_{11} was observed to undergo slower aging than the irradiated devices and ultimately exhibited the highest output voltage at the end of the aging study.

4.8 Quantum Efficiency of InP QD-PPDs

In an ideal polymer photodetector, all photons incident on the detector would be absorbed and would efficiently create electron-hole pairs all of which would reach the device electrodes. In reality, the investigation of polymer photodetectors fabricated in this study are far from ideal and, based on the data presented it is suggested that most of the photon-generated electron–hole pairs undergo significant recombination. Thus, the current flow experienced in an external circuit (load resistance) for a less than ideal PPD will not surprisingly be quite small. This is precisely the situation for the QD PPDs fabricated and investigated in this study. As evidenced by the data generated during the proton irradiation of InP QD PPDs, significant deterioration of the device photovoltage output response suggests corresponding reduction in carrier populations which in turn directly reduce the device quantum efficiency. The external quantum efficiency calculations that follow are presented for completeness and to provide a benchmark for future investigations.

The external quantum efficiency (η) of a polymer photodetector illuminated by monochromatic light of wavelength (λ) can be expressed as:

$$\eta = \frac{\text{Photocurrent Density (electrons per unit area and time).}}{\text{Light Intensity (photons per unit area and time)}} \quad (3)$$

The ratio shown in Equation (3) is commonly referred to as the incident photon-to-current conversion efficiency (IPCE), where:

$$\text{IPCE (\%)} = 1240\, J_\lambda / \lambda\, P_\lambda. \quad (4)$$

In equation (4), J_λ represents the PPD short circuit current expressed in mA/cm^2, λ is expressed in nm, and P_λ is the light intensity incident on the PPD expressed in W/m^2 [6].

As discussed earlier in Section 3.3, a non-irradiated InP QD-sensitized HTM-TiO_2 hybrid PPD (shown in Figure 10) was determined to have an IPCE of 0.007% when illuminated by a laser operating at λ = 532 nm. It is of interest to compare the IPCE of the non-irradiated device

with the IPCE calculated for sample P_{10}, irradiated by protons to a total dose of 150 krad(Si). The InP QD PPD P_{10} sample exhibited a short circuit current of 1.5 μA at λ = 500 nm when illuminated by the solar simulator operating at 2.745 mW. A maximum open circuit photovoltage was measured at 297.31mV (Figure 35) by illuminating the PPD over an area of 0.28 cm^2. According to Equation (4), the IPCE for the P_{10} sample can be calculated as follows:

$$\text{IPCE (\%)} = \frac{1240\ (1.5\text{x}10^{-3}\ \text{mA} / 0.28\ \text{cm}^2)}{[500\ (2.745\text{x}10^{-3}\ \text{W} / 0.28\text{x}10^{-4}\ \text{m}^2)]} \qquad (5)$$

$$\text{IPCE (\%)} = 0.014\ \%. \qquad (6)$$

As can be seen, the external quantum efficiency (0.014 %) for the irradiated InP QD PPD exceeds that of the non-irradiated device (0.007 %). However, caution must be taken in comparing and interpreting these results. The light intensity of the laser far exceeded that of the solar simulator by two orders of magnitude, the measurements were not made at the same wavelength nor were equivalent areas illuminated by the two sources. What is remarkable is that the calculations suggest that the IPCE of the InP QD PPD was not severely affected by proton irradiation at 150 krad(Si). This empirical data again confirmed that the InP QD PPDs exhibited excellent resistance to gamma-ray and high energy proton irradiations.

4.9 CdSe QD PPD Pre- and Post- Proton Irradiation Reponses

CdSe QDs and materials have attracted much interest in the potential development of photonic devices however, publications regarding the radiation resistance of the material or which investigate specific applications are scarce [32]. As such, the empirical data resulting from the IPC and NS investigations is of particular importance and provides a first indication of the extent of radiation resistance in CdSe QD PPDs.

TEM imaging of the QD liquid suspension revealed uniform spherical QD sizes of ~ 4nm. Figure 50 shows the optical absorption of the CdSe solution and that of the active TiO_2/CdSe film. As can be observed, the CdSe QD in solution indicates substantial

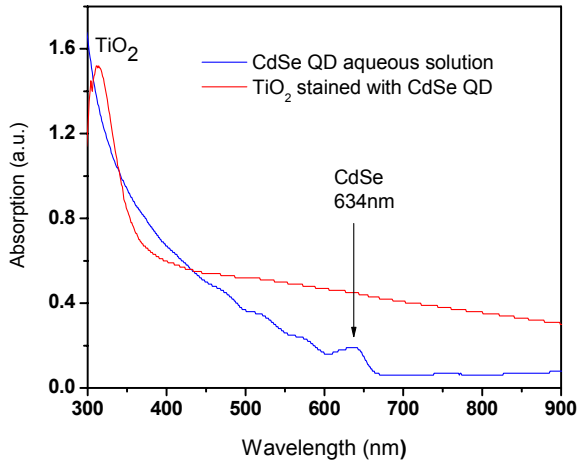

Figure 50. Optical absorption of CdSe QD solution and CdSe-stained TiO_2 film.

absorption in the near- IR relative to lower wavelengths but decreases substantially when prepared as a solid film. The QDs were obtained from a commercial source and were used to stain the porous TiO_2 film which was deposited onto an ITO/anatase and TiO_2-coated glass substrate. This process was followed by deposition of the polymer HTM onto the layered film. The HTM consisted of the same components and concentrations as used in the fabrication of InP QD PPDs. Using vacuum deposition, aluminum counter-electrodes 200 nm thick were deposited onto the active film.

As in previous photovoltage response measurements, a wavelength-filtered solar simulator was used to illuminate the PPDs at incremental and discreet wavelengths for conducting pre-and post-irradiation measurements of the PPD photovoltage output responses. Each CdSe QD PPD device was illuminated for a period of 8 seconds over an active area of 0.28 cm^2 and at the same solar simulator intensity as previously used in the InP QD PPD studies. Figure 51 shows a typical CdSe QD PPD (sample 5) exhibiting a maximum photovoltage output of 392.1 mV at λ =600 nm when illuminated for 8 seconds.

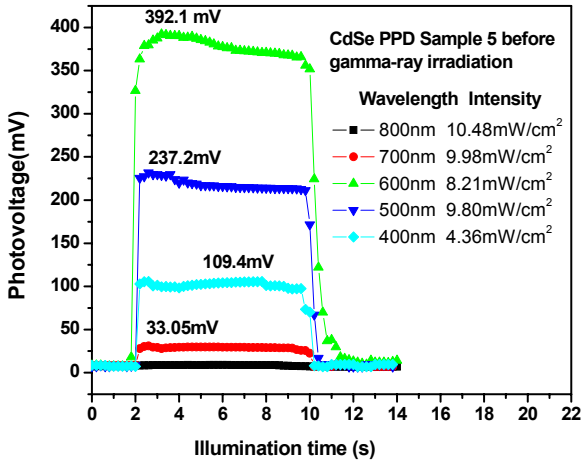

Figure 51. Typical pre-irradiation open circuit photovoltage of CdSe QD PPD. Photovoltage responses at discreet wavelengths are shown for 8 s illuminations of CdSe QD PPD sample 5.

Illumination intensities previously used in the InP QD PPD gamma-ray studies were again applied for the CdSe QD PPD studies. Table 6 summarizes the photovoltage outputs and short-circuit currents generated by the CdSe QD PPDs illuminated at $\lambda = 600$ nm.

Table 6. CdSe QD PPD pre- and post- gamma-ray irradiation responses

CdSe PPD Sample	*D_γ [krad(Si)]	$PV_{(pre\text{-}irrad.)}$ [mV]	$PV_{(post\text{-}irrad.)}$ [mV]	ΔPV [mV]	$I_{sc\ (pre\text{-}irrad.)}$ [μA]	$IPCE_{(pre\text{-}irrad.)}$ [%]	**$I_{sc\ (post\text{-}irrad.)}$ [μA]
13 (control)	0	328.3	109.4	218.7	9.3	0.084	None
10 (control)	0	352.7	136.6	216.1	11.7	0.105	None
1	10.5	319.8	106.9	212.9	5.9	0.053	None
4	10.5	308.3	84.22	224.1	7.1	0.064	None
3	51.6	375.2	117.4	257.8	10.2	0.092	None
8	51.6	318.9	73.32	245.6	8.5	0.077	None
14	94.3	374.5	106.2	268.3	9.4	0.085	None
7	94.3	304.2	53.14	251.1	6.8	0.061	None
5	153	390.2	33.06	356.6	12.3	0.110	None
12	153	316.3	38.16	278.1	7.6	0.068	None

* Average dose rate of 121 rad(Si) min^{-1}
*High noise levels prevented measurement of the short circuit current.

The pre- and post-irradiation photovoltage data [$PV_{(pre\text{-}irrad.)}$ and $PV_{(post\text{-}irrad.)}$, respectively] as well as the pre- and post- short circuit currents [$I_{sc(pre\text{-}irrad.)}$ and $I_{sc(post\text{-}\ irrad.)}$, respectively] for each PPD sample were the averaged data of four individual areas on the PPD array. A ~ 6% uncertainty in the measurements was attributed to ambient light and electrical

contact noise. The data were obtained at λ = 600nm with an illumination time of 8 seconds and an illumination spot size incident on each PPD array element of 0.28 cm^2 at a power density of 8.21mW/cm^2.

The post– irradiation external quantum efficiency was not calculated and tabulated in Table 5 since $I_{sc(post\text{-}irrad.)}$ in all devices were seriously deteriorated prior to the irradiation. The deterioration was attributed to aggressive aging within all samples. In Table 6, ΔPV represents the post-irradiation photovoltage which included reduced photovoltage from aggressive aging and a reduction of the photovoltage due to the irradiation process. As can be seen the non-irradiated control devices experience an average aging loss of ~ 214.4 mV.

Shown in Figure 52 are the effects of aging exhibited by two non-irradiated control CdSe QD PPDs (samples 13 and 10). As may be observed there were significant decreases in the photovoltage outputs following their fabrication and photovoltage outputs, one month previously.

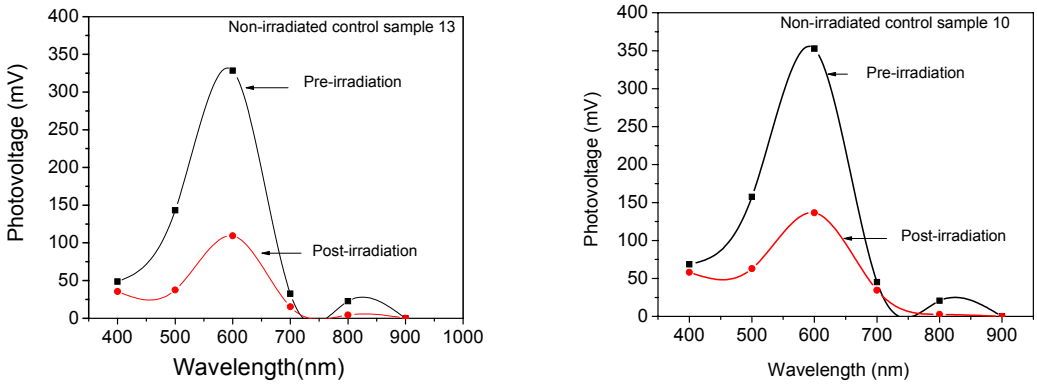

Figure 52. Aging of two non-irradiated CdSe QD PPD control samples. Deterioration of two control device photovoltage outputs over a period of one month is shown. Top response curves represent pre-irradiation measurements and the lower curves were responses measured following PPD post-irradiation measurements.

Figures 53 – 55 show the results of irradiated devices (1, 4), (3, 8) and (14, 7) irradiated

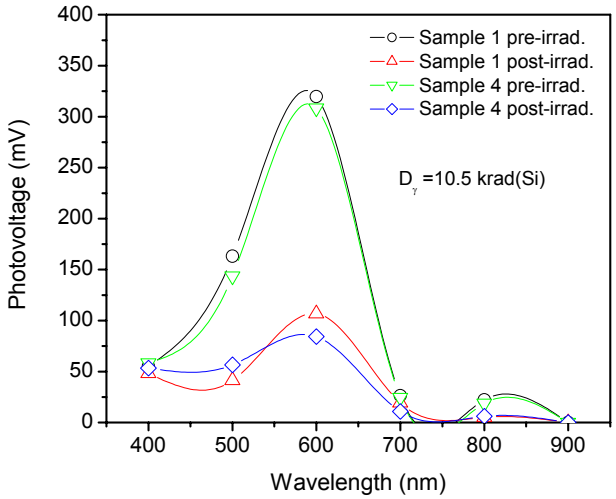

Figure 53. Photovoltages of gamma-ray irradiated CdSe QD PPDs 1 and 4.

at doses of 10.5, 51.6 and 94.3 krad(Si), respectively. The irradiated device photovoltage responses were very similar to the photovoltage output decreases observed in the non-irradiated control devices confirming that there was no significant gamma-ray induced damage experienced by the CD QD PPDs at low dose.

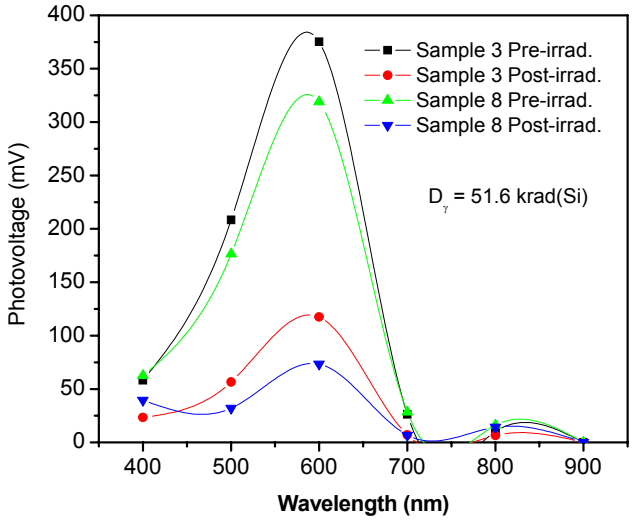

Figure 54. Photovoltages of gamma-ray irradiated CdSe QD PPDs 3 and 8.

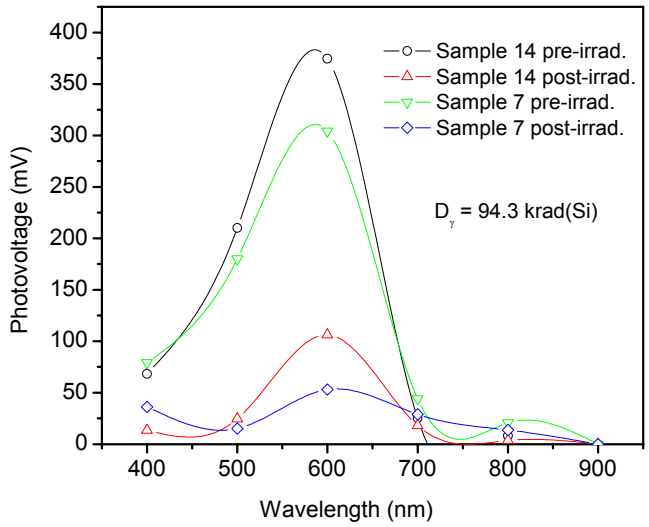

Figure 55. Photovoltages of gamma-ray irradiated CdSe QD PPDs 14 and 7.

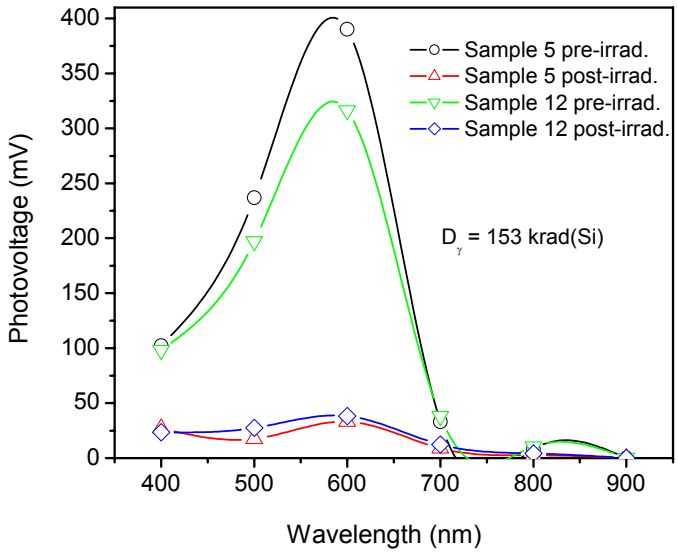

Figure 56. Photovoltages of gamma-ray irradiated CdSe QD PPDs 5 and 12.

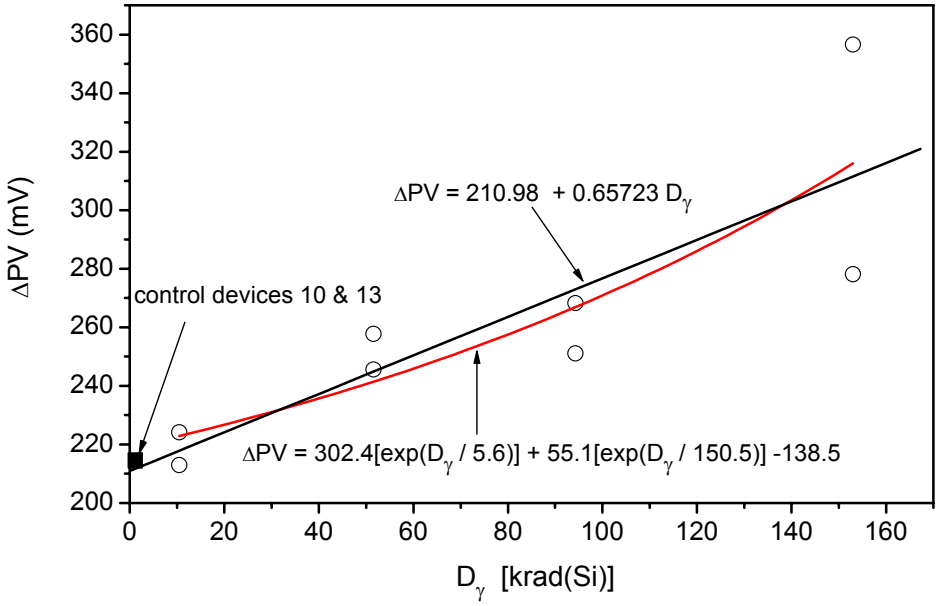

Figure 57. Photovoltage responses of gamma-ray irradiated CdSe QD PPDs at λ = 600 nm. The CdSe QD PPDs exhibited excellent resistance to gamma- rays to a total dose of ~ 150 krad(Si). Both linear and a second order exponential curve fit the data. The decrease in photovoltage is largely attributed to aging effects experienced before the irradiations.

Linear (R^2 = .95) and second order exponential (R^2 = 0.85) curve fits are shown for the decrease in the irradiated CdSe QD PPD photovoltages as a function of applied dose. At doses < 94.3krad(Si) the decrease in the photovoltage outputs were elevated to ~ 23 % above the photovoltage decreases noted in the two non-irradiated control devices, while at a D_γ = 153 krad(Si) the increase relative to the control devices was 39 %.

A comparison of InP QD PPD response data (Figure 13) with CdSe QD PPD data (Figure 57) PV- from the theoretical ΔPV linear curve fits shows damage coefficients of 1.64 mV/krad(si) and 0.657 mV/krad(Si), respectively (i.e.: a ratio of 2.5 : 1). This ratio suggests that the CdSe QD exhibited greater resistance to gamma-rays compared to the InP QD PPDs over the same dose range. It is important to consider that the InP QD PPD PV responses were made using a 532 nm laser source, while the CdSe QD PPDs responses were measured with a solar simulator operating at λ = 600 nm. It is not believed that the differences noted in either wavelength or illumination conditions should affect the linear curve slopes determined by the PV responses. Under these assumptions,

the CdSe QD PPDs appear to exhibit greater resistance to gamma-rays compared to the InP QD PPDs.

As explained previously for similar post-irradiation photovoltage measurements in InP QD PPDS, a known component contributing to the reduction in photovoltage is attributed to the loss of light intensity [estimated at ~ 6 % at a gamma-ray dose of ~150 krad(Si)] in reaching the PPD active area. This is caused by the radiation induced absorption in the borosilicate glass substrate at λ = 600 nm. The data shown in Figure 51 and Figures 53-57 are not compensated for gamma-ray induced absorption losses in the substrate.

Pre-irradiation measurements of the short circuit current measurements ranged from 5.9 to 12.3 μA, however, short circuit current levels in the irradiated PPDs including the non-irradiated control samples measured later in time were below the signal/noise resolution of the measurement system. The large increase in the current noise level and suppressed short circuit current was attributed to rapid aging effects in the PPDs and not as a consequence of the irradiations. Approximately one month elapsed between the device fabrication, photovoltage and short circuit current measurements, and, the post- gamma-ray irradiation measurements. The control CdSe QD PPDs experienced significant aging decay in this short interval resulting in photovoltage decreases of 66.5% and 63.9 % as measured in the two control devices.

Compared to the performance of the InP QD PPD devices, the CdSe QD PPD devices were quite unstable. However, the external quantum efficiencies of the pre-irradiated CdSe QD detectors were much higher compared to InP QD detectors. The gamma-ray damage constant for CdSe QD PPDs compared to that of InP QD PPDs is lower by a factor of 2.5, indicating that that the CdSe QD PPDs exhibited greater resistance to gamma-ray irradiations.

5.0 CONCLUSIONS

Polymer photovoltaic detectors incorporating InP QDs exhibited higher open circuit photovoltages and responded further into the near-IR compared to polymer photovoltaic detectors based on CdSe QDs.

Excellent peak photovoltage responses for sixteen pre-irradiated InP QD PPDs under laser illumination at λ = 532 nm and 245 mW incident power, ranged from 307-617 mV, while illumination of ten CdSe QD PPDs using a solar simulator yielded photovoltages ranging from 304 - 309 mV (8.21 mW/cm^2 at λ = 600 nm), and , 22.7 mV at 900 nm (40.5 mW/cm^2 incident power).

InP QD PPDs exhibited near-IR responses to ~ 1000 nm, while the CdSe QD PPDs cut-off at ~ 700 nm. The study was successful in demonstrating that QDs introduced within the polymer matrix shift the detector absorption spectra towards the near-IR. The QD sizes ranged from ~ 2-10 nm for InP QDs and ~ 4 nm for CdSe QDs.

Aging studies performed on irradiated InP QD PPDs suggest that trap filling and photobleaching processes assist in mitigating the transient and long term gamma-ray induced reduction of photovoltage signal. While it could not be directly determined from the irradiation results, localization of the exciton field by the introduction of QDs into the polymer matrix was believed to reduce the non-radiative recombination processes within the QD PPDs and contributed to the observed radiation resistance of the detectors. Room temperature annealing and the diffusion of deep traps under broadband illumination was observed to be time dependent. A study varying the parameters of QD size, and concentration, would be required to ascertain the exact role that QDs play in the radiation resistance of QD PPDs. These results were also believed duplicative for the CdSe QD PPDs.

Following irradiation of InP QD PPDs by energetic protons (i.e. 25.6 MeV) aging studies conducted under conditions similar to the gamma-ray post-irradiation aging studies

suggested that trap filling and photobleaching processes were greatly reduced. Energetic protons were believed responsible for considerable dislocation damage in or near the interface of the active HTM- TiO_2 heterojunction.

At a dose of ~150 krad(Si) the presence of very small decays following irradiation by gamma-rays and protons suggest that the HTM polymer may have sustained substantial damage. If so, regeneration of the charge carriers would be impeded. The possibility that degradation to the TiO_2 and InP QDs materials also occurred cannot be dismissed, however based on other radiation effects studies performed on QDs, it may be prudent to assert that the QDs were probably the least affected. An independent study of the effects of radiation on the QDs, TiO_2-electron acceptor and the polymer hole transport material would be required to differentiate the extent of degradation experienced by each of the components comprising the PPD.

The relative radiation resistance exhibited by InP and CdSe QD devices was successfully measured and demonstrated that InP QD PPDs showed excellent resistance to gamma-ray and protons (25.6 Mev. 10^{11} p+/cm^2) at a total dose of ~ 150 krad(Si), while CdSe QD PPDs irradiated by gamma-rays to ~ 152 krad(Si) appeared to have damaged more from environmentally –induced aging effects rather than via ionization-induced processes. The data suggest that both InP and CdSe based polymer detectors have excellent resistance to gamma-ray and energetic protons to a total dose of ~150 krad(Si).

These and other valuable empirical data acquired during the investigation demonstrated a high potential for developing radiation resistant QD PPDs suitable for space applications. Development of reliable, radiation resistant polymer based detectors operating over visible, near- IR and mid- IR wavelengths will undoubtedly find widespread use in space system applications.

6.0 RECOMMENDATIONS

The investigation and development of radiation resistant polymer–based photovoltaic detectors for eventual use as near-IR photodetectors in space applications was highly

successful. Specific recommendations for advancing the technology to the next level of development are offered with the understanding that the investigative results assimilated by IPC and NS are empirical and several years of concentrated effort will be required to develop a device capable of reliable and hardened operation in the space environment. Areas of recommended research and development critical to further advancement of the technology are shown in prioritized order.

Develop improved processing techniques for controlling the size and distribution of QD ensembles. While the results of the IPC and NS investigation showed that the absorption spectra of the QD-doped PPDs could be shifted to near-IR wavelengths, the QD number densities for sizes larger than 6 nm necessary to achieve red-shifts was far from optimum. This was also true for the CdSe QDs that only averaged 4 nm in size and showed less red shift then that of the InP QDs. Higher concentrations of QDs and larger sizes are required to improve the absorption and potentially the quantum efficiency of the QD –based PPDs.

- Recommend that a follow on study to improve the size, shape and distribution of InP and CdSe QDs be undertaken for the purpose of improving the QD optical absorption and shifting the PPD response beyond 1000 nm .

Conduct in situ irradiations of QD PPDs. Passive irradiations such as those performed in this study provide an economical means for conducting radiation effects investigations of QD PPDs. However, time resolved in situ irradiation studies conducted on an operational QD PPD will reveal important transient phenomena that may be used to differentiate important parameters such as carrier recombination rates, exciton lifetimes, annealing rates, charge transport processes and other dynamic measurements not possible using post-irradiation data gained from passive irradiations. Response data acquired under in situ conditions would help to elucidate the underpinnings of the light-matter –ionization interaction physics of QD PPDs which is required to develop efficient and radiation hard devices capable of reliable operation in the near- and mid IR.

- Recommend that a follow-on in situ irradiation study be enjoined to thoroughly exploit the merits and allow a deeper understanding of the interaction kinetics in QD PPDs.

Investigate and quantify the extent of ionization and dislocation induced effects in key inorganic and organic components. A successfully completed objective of the IPC and NS investigation reported herein was to determine the radiation resistance of fabricated QD PPDs. While it was demonstrated that InP and CdSe QD PPDs exhibit excellent radiation resistance to 150 krad(Si), little is known of the effects of radiation on the individual components comprising the PPD or the responses of these components at higher dose. Quantification of the component damage coefficients will accelerate improving the radiation resistance beyond current dose levels and will increase the potential for near-term applications in space and strategic systems.

- Recommend that a follow-on study for determining and quantifying the effects of ionizing radiation on: InP and CdSe QDs, spiro-OMeTAD, TiO_2-nanocrystals, and, other emerging QDs, electron acceptor and hole transport materials be undertaken to specifically identify their radiation resistance.

Determine specific components of the natural aging process and accelerated aging resulting from electrons and proton irradiations. The environmental stability of polymer based detectors is not well known and less is known of their stability under irradiation by high energy charged particles. These are critical issues requiring resolution prior to using PPDs in space applications. The investigative results reported herein have provided indications that aging effects are affected by gamma-ray and proton irradiation, but the determination of the exact nature of the interactions were beyond the scope of the effort.

- Recommend that a follow-on study for determining the effects of ionizing radiation on the stability and aging tendencies of QD PPDs be undertaken to specifically identify and quantify the effects that native defects and residual polymer-chemical agents within the PPD present when interacting with the

ambient environment and ionizing radiation. Since it suggested from the data herein that these defects and agents may act as precursors in altering the aging process, a thorough study to differentiate the interaction kinetics are recommended. Additionally recommend that investigation of chemical stabilizers (e.g. antioxidants) be investigated as a means for stabilizing or mitigating the aging process. Recommend the role of photobleaching be thoroughly investigated.

Identify and develop thin–radiation resistant substrates for QD PPDs. Currently borosilicate glass is used as a transparent PPD substrate material, which damages during exposure to ionizing irradiation. An appropriate radiation resistant substrate material should be developed that would provide the necessary structure and adhesion for bonding to the PPDs , while resisting radiation damage.

- Recommend that polymer substrates rather than glass substrates be used in QD PPD devices. Numerous thin film flexible substrates such as poly(methyl methacrylate) exhibit good transparency, stability and radiation resistance.

Identify and investigate new and emerging QD materials for improving PPD performance. The IPC and NS approach for developing next–generation PPDs is unique in that the eventual selection of an optimum QD sensitizer will be selected for its ability to absorb in the near to mid-IR while exhibiting superior resistance to space environments such as electrons.

- Recommend that continual identification and investigation of new and promising QD materials be an integral component to any follow-on efforts.

REFERENCES

[1] E. W. Taylor, "Investigation of radiation resistant polymer photodetectors for space applications" AFRL-VS-TR-2002-1105, (11 September 2002).

[2] E. W. Taylor, D. Le, M. F. Durstock, B. E. Taylor, R. O. Claus, T. Zeng, C. P. Morath, D. Cardimona, "Space radiation induced effects in polymer photo-detectors", Proc. SPIE ,**4128,** (July, 2002).

[3] C. B. Murray, D. J. Norris, and M. G. Bawendi, "Synthesis and characterization of nearly monodisperse CdE (E= S, Se, Te) semiconductor nanocrystallites", J. Amer. Chem. Soc., **115**, 8706, (1993).

[4] Z. A. Peng and X. Peng, "Formation of high quality CdTe, CdSe, and CdS nanocrystals using CdO as a precursor", J. of Amer. Chem. Soc., **123**, 183, (2001).

[5] O. I. Micic, H. M. Cheong, H. Fu, A. Zunger, J. R. Sprague, A. Mascarenhas and A. J. Nozik, "Size-dependent spectroscopy of InP quantum dots", J. Phys. Chem. B, **101**, 4904, (1997).

[6] Craig R. Rice, Michael D. Ward, Mohammed K. Nazeeruddin and Michael Grätzel, New J. Chem., **24,** 651, (2000).

[7] O. I. Micic, A. J. Nozik, "Synthesis and characterization of binary and ternary III-V quantum dots" J. Luminescence, **70**, 107, (1966).

[8] A. A. Guzelian, J. E. B. Katari, A. V. Kadavanich, U. Banin, K. Hamad, A.P. Alivisatos, R. H. Wolters, C. C. Arnold, J. R. Heath, "Synthesis of size-selected, surface–passivated InP nanocrystals", J. Phys. Chem., **100**, 7212, (1996).

[9] H. Fu, A. Zunger, "Excitons in InP quantum dots", Phys. Rev, B, **57**, No. 24, R15064, (15 June 1998).

[10] E. W. Taylor, J. Nichter, F. Nash, R. Michalak, F. Haas, P. Payson, P. Cook, T. McEwen, B. McKeon, A. Szep, B. Flushe, A. Pirich, G. Brost, J. Grote, J. Zetts, P. Yaney, E. Heckman "Behavior of NLO polymer modulators irradiated by gamma-rays", SPIE, **5212**, (7 August 2003).

[11] E. W. Taylor, R. Claus, K. Cooper, L. R. Taylor, "Gamma-ray irradiation and responses of electrostatically assembled electro optic polymer materials", SPIE, **4547**, (17-21, September 2001).

[12] E. W. Taylor. "Inorganic and polymer photonic sensor technologies in space missions", Proc. 18th IEEE Instrumentation and Measurement Technology Conference, **3**, ISBN 0-7803-6646-8, (21-23 May 2001).

[13] E. W. Taylor, *"Radiation Effects",* Chapter 14.1, in: Properties of Lithium Niobate**,** Edited by K.K. Wong , IEE EMIS Datareviews Series, No. 28, 359, (2002).

[14] E. W. Taylor, J. Grote, J. Zetts, J.E. Winter , A. D. Sanchez , D. Craig, "In situ high energy proton irradiation of nonlinear organic modulator materials for space environments"**,** SPIE, **4134**, (1 August 2000).

[15] J. Grote, E. W. Taylor, J. Zetts, J. Winter, A. D. Sanchez, D. Craig, F. Hopkins, "Optical transmission and thermal heating effects due to irradiation of nonlinear optic and conductive polymers for spaced based electrooptic applications", SPIE, **4134**, San Diego, CA, (1 August 2000).

[16] S. Kirshna, S. Raghavan, G. von Winckel, P. Rotella, A. Stintz, C. P. Morath, D. Le, S. W. Kennerly, "Two color InAS/InGaAs dots-in-a-well detector with background-limited performance at 91 K", App. Phys. Lett., **82**, No. 16, (21 April 2003).

[17] W. V. Schoenfeld, C. H-. Chen, P. M. Petroff and E. L. Hu, "Argon ion damage in self-assembled quantum dots and structures", Appl. Phys. Lett., **73**, No. 20, 2935, (16 November 1998).

[18] R. Leon, G.W. Swift, B. Magness, W. A. Taylor, Y. S. Yang, K. L. Wang, P. Dowd, Y. H. Zhang, "Changes in luminescence emission by proton irradiation: InGa/GaAs quantum wells and quantum dots, "Appl. Phys. Lett. **76**, No. 15, 2074, (10 April 2000).

[19] F. Guffarth, R. Heitz, M. Geller, C. Kapteyn, H. Born, R. Sellin, A. Hoffmann, D. Bimberg, N. A. Sobolev, M. C. Carmo, "Radiation hardness of InGaAs/GaAs quantum dots", Appl. Phys. Lett., **82**, No.12, 1941, (24 March 2003).

[20} R. Leon, S. Marcinkevicius, J. Siegert, B. Cechavicius, B. Magness, W. Taylor, C. Lobo, "Effects of proton irradiation on luminescence emission and carrier dynamics of self-assembled III-V quantum dots", IEEE Trans. Nuc. Sci., **49**, No. 6, 2844, (6 December 2002).

[21] C. Ribbat, R. Sellin, M. Grundemann, D. Bimberg, N. A. Sobloev, M. C. Carmo, "Enhanced radiation hardness of quantum dot lasers to high energy proton irradiation", Electron. Lett., **82**, No. 12, 1941, (24 March 03).

[22] "Standard Practice for Minimizing Dosimetry Errors in Radiation Hardness Testing of Silicon Devices Using Co-60 Sources", ASTM Committee E10.07 on Nuclear Technology and Applications, Designation: E 1249-00, (July, 2000).

[23] E. W. Taylor, K. L. Cooper, R. O. Claus, L. R. Taylor, "Gamma-ray irradiation and responses of electronically assembled electro-optic polymer materials", SPIE, **4547**, (September 2001).

[24] E. W. Taylor, A. D. Sanchez, S. P. Chapman, S. A. DeWalt, D. M. Craig, M. A. Kelly, M. F. Mitcham, "Responses of a spatial light modulator to pulsed electrons", OSA Technical Digest, **9**, (14 March 1995).

[25] Origin Scientific Graphing and Analysis, Version 7.

[26] J. Suski, J. C. Bourgin, "Defects introduced by electron irradiation in InP", J. Appl. Phys., **54**, No.5, 2852, (May 1983).

[27] M. Yamaguchi, C. Uemura, K. Ando, "Radiation damage in InP single crystals and solar cells", J. Appl. Phys. **55**, No.6, 1429, (1 November 1983).

[28] M. Yamaguchi, K. Ando, C. Uemura, "Carrier concentration effects on radiation damage in InP", J. Appl. Phys. **55**, 3160, (15 April 1984).

[29] M. Yamaguchi, Y. Yoshio, K. Ando, "Room–temperature annealing of radiation-induced defects in InP solar cells", Appl. Phys. Lett., **45**, No.11, 1206, (1 December 1984).

[30] M. Yamaguchi, K. Ando, "Mechanism for radiation resistance of InP solar cells", J. Appl. Phys., **63**, No. 11, 5555, (1 June 1998).

[31] J. F. Zigler, J. P. Biersack, U. Littmark, The Stopping and Ion Range of Ions in Matter, Pergamon, New York (1985).

[32] L. Zhang, F. Zhang, Y. Wang, R. O. Claus, "Linear electro-optic tensor ratio determination and quadratic electro-optic modulation of electrostatically self-assembled CdSe quantum dot films", J. Chem. Phys., **116**, No.14, 6297, (8 April 2004).

DISTRIBUTION LIST

DTIC/OCP
8725 John J. Kingman Rd, Suite 0944
Ft Belvoir, VA 22060-6218 1 cy

AFRL/VSIL
Kirtland AFB, NM 87117-5776 1 cy

AFRL/VSIH
Kirtland AFB, NM 87117-5776 1 cy

International Photonics Consultants, Inc.
38 Knife Edge
Pagosa Springs, CO 81147 1 cy

Official Record Copy
AFRL/VSSS/Capt Dang Le 1 cy